

# UC Santa Cruz

## UC Santa Cruz Previously Published Works

### Title

Human calpain-3 and its structural plasticity: Dissociation of a homohexamer into dimers on binding titin.

### Permalink

<https://escholarship.org/uc/item/9329g06d>

### Journal

Journal of Biological Chemistry, 301(2)

### Authors

Ye, Qilu

Henrickson, Amy

Demeler, Borries

et al.

### Publication Date

2024-12-24

### DOI

10.1016/j.jbc.2024.108133

Peer reviewed



# Human calpain-3 and its structural plasticity: Dissociation of a homohexamer into dimers on binding titin

Received for publication, October 29, 2024, and in revised form, December 17, 2024. Published, Papers in Press, December 24, 2024.  
<https://doi.org/10.1016/j.jbc.2024.108133>

Qilu Ye<sup>1</sup>, Amy Henrickson<sup>2</sup>, Borries Demeler<sup>2</sup> , Vitor Hugo Balasco Serrão<sup>3,4</sup> , and Peter L. Davies<sup>1,\*</sup>

From the <sup>1</sup>Department of Biomedical and Molecular Sciences, Queen's University, Kingston, Ontario, Canada; <sup>2</sup>Department of Chemistry & Biochemistry, University of Lethbridge, Lethbridge, Alberta, Canada; <sup>3</sup>Biomolecular Cryo-Electron Microscopy Facility, and <sup>4</sup>Department of Chemistry and Biochemistry, University of California - Santa Cruz, Santa Cruz, California, United States

Reviewed by members of the JBC Editorial Board. Edited by Wolfgang Peti

Calpain-3 is an intracellular Ca<sup>2+</sup>-dependent cysteine protease abundant in skeletal muscle. Loss-of-function mutations in its single-copy gene cause a dystrophy of the limb-girdle muscles. These mutations, of which there are over 500 in humans, are spread all along this 94-kDa multidomain protein that includes three 40+-residue sequences (NS, IS1, and IS2). The latter sequences are unique to this calpain isoform and are hypersensitive to proteolysis. To investigate the whole enzyme structure and how mutations might affect its activity, we produced the proteolytically more stable 85-kDa calpain-3 ΔNS ΔIS1 form with a C129A inactivating mutation as a recombinant protein in *Escherichia coli*. During size-exclusion chromatography, this calpain-3 was consistently eluted as a much larger 0.5-MDa complex rather than the expected 170-kDa dimer. Its size, which was confirmed by SEC-MALS, Blue Native PAGE, and AUC, made the complex amenable to single-particle cryo-EM analysis. From two data sets, we obtained a 3.85-Å reconstruction map that shows the complex is a trimer of calpain-3 dimers with six penta-EF-hand domains at its core. Calpain-3 has been reported to bind the N2A region of the giant muscle protein titin. When this 37-kDa region of titin was co-expressed with calpain-3, the multimer was reduced to a 320-kDa particle, which appears to be the calpain dimer bound to several copies of the titin fragment. We suggest that newly synthesized calpain-3 is kept as an inactive hexamer until it binds the N2A region of titin in the sarcomere, whereupon it dissociates into functional dimers.

The calpain superfamily is comprised of Ca<sup>2+</sup>-dependent, intracellular, cysteine proteases (1–3). These multidomain enzymes are tightly regulated and perform limited cleavage of their target proteins to help initiate cellular processes including cell motility, signal transduction, cell cycle progression, apoptosis, and gene expression. Abnormal regulation of calpain proteases has been correlated with various diseases such as neurodegenerative disorders, various cancers, cardiovascular disorders, muscular dystrophy, metabolic diseases, and inflammation among others (4–6). In mammals, the calpain family is composed of 15 gene products, nine of which are

ubiquitously expressed while six have been found to be tissue-specific based on their gene expression profiles and physiological roles (7). Calpain-3 is in the latter category and is predominantly expressed in skeletal muscle (8). Soon after the discovery of this muscle-specific family member, inactivating mutations in the calpain-3 gene (*CAPN3*) were shown to cause the autosomal recessive form of limb girdle muscular dystrophy type R1 (LGMDR1) (9). The physiological functions of calpain-3 are thought to include the natural turnover of muscle proteins (10, 11), regulation of calcium release and recruitment of binding partners in skeletal muscle (12), and remodeling of the sarcomere upon exercise stress, especially after eccentric exercise (13, 14). However, the precise mechanism by which calpain-3 functions in the physiology of healthy muscle and LGMDR1 pathogenesis remains unclear.

Calpain-1 and -2 are designated as “conventional calpains” and were the first members of the calpain superfamily to have been purified and characterized (1). Conventional calpains have a heterodimeric architecture (Fig. 1), composed of a catalytic large 80 kDa subunit and a regulatory small 28 kDa subunit, both of which are required for function (15). The catalytic large subunit contains an N-terminal anchor helix and four domains: the calpain-type cysteine protease core domains PC1 (containing the catalytic cysteine) and PC2 (containing histidine and asparagine, which together form a catalytic triad upon calcium binding) (16), the calpain-type beta-sandwich (CBSW) domain, and the penta-EF-hand (PEF(L), where L indicates large subunit) domain (3). The small subunit of calpain contains a glycine-rich region and a PEF(S) (where S indicates small subunit) domain that serves a regulatory function. Each PEF(L) and PEF(S) domain contain five EF-hand α-helical motifs which fold together to form pairs: EF1 with EF2, EF3 with EF4, while EF5 is unpaired. The EF5 from each of PEF(L) and PEF(S) domains pair up with each other to form a heterodimer. This interaction is stabilized through a short antiparallel beta-sheet, with contributions from some hydrophobic interactions (17–20). The same fifth EF-hand pairing of the homodimeric and heterodimeric PEF domains takes place whether Ca<sup>2+</sup> is present or absent.

The domain architecture of calpain-3 is similar to that of the large subunit of conventional calpains, being comprised of the protease core domains PC1 and PC2, the CBSW domain, as

\* For correspondence: Peter L. Davies, [daviesp@queensu.ca](mailto:daviesp@queensu.ca).

## Calpain-3 homohexamer dissociates to dimers on binding titin

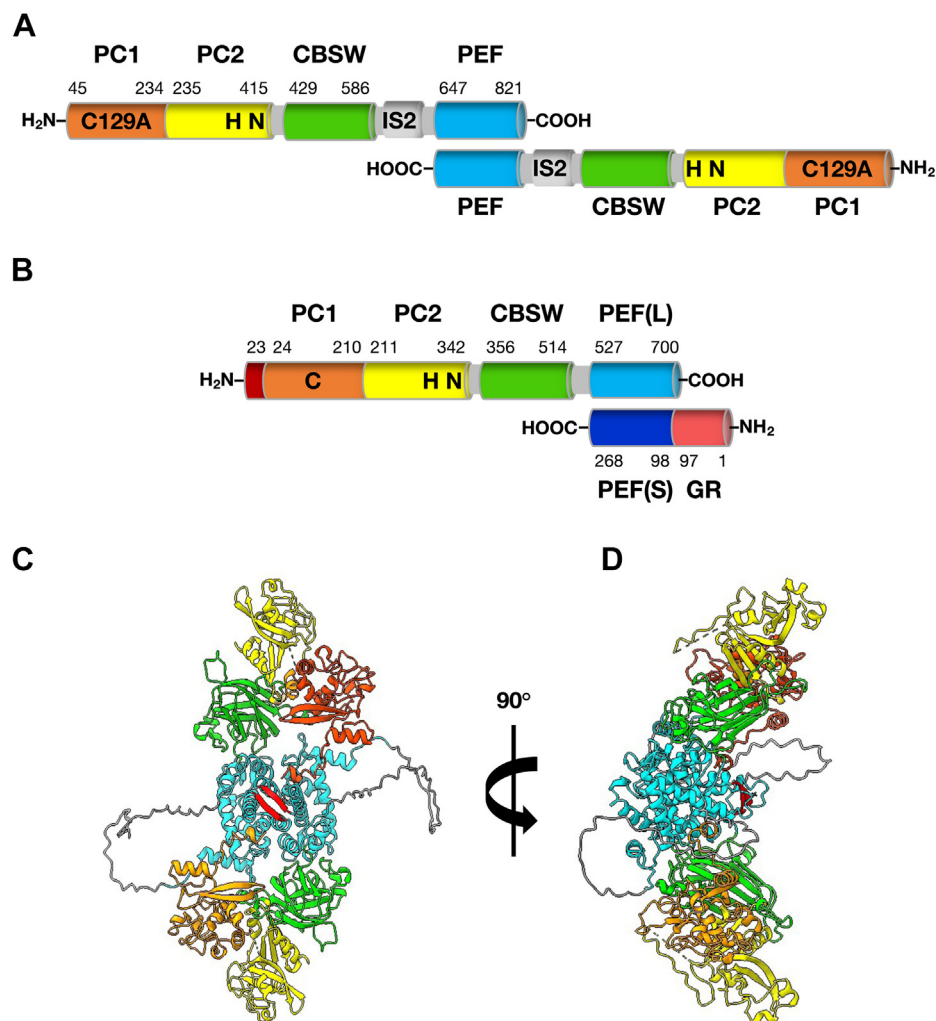


**Figure 1. AlphaFold2 homodimer structure of calpain-3 (C129A)  $\Delta$ NS&IS1.** A, domain map of calpain-3 (C129A)  $\Delta$ NS&IS1 homodimer paired antiparallel through the PEF domains. B, domain map of calpain-2 heterodimer paired antiparallel through the PEF domains of the large and small subunits. C and D, ribbon diagram of the dimer structure of calpain-3 lacking NS and IS1 but with the IS2 present viewed from the front and side, respectively. Orange and yellow ribbons represent protease core domains, PC1 and PC2, respectively. The CBSW domain is green, and the PEF domain is shown in cyan. IS2 is colored gray, and red ribbons indicate paired EF5 motifs from the two calpain-3 molecules in the dimer.

well as a C-terminal PEF domain (Fig. 1) (21). A sequence comparison indicates that calpain-3 shares approximately 51% and 54% sequence identity with the large subunit in conventional calpain-1 and calpain-2, respectively, but contains three additional sequences that are unique to calpain-3. These are an N-terminal sequence (NS) at the very N-terminal end, preceding PC1; an insertion sequence 1 (IS1) located in protease core domain PC2; and an insertion sequence 2 (IS2) situated between the CBSW domain and the PEF domain (22, 23). These three additional regions confer unique physiological functions to calpain-3 distinct from the conventional calpains but also predispose it to rapid proteolysis. The half-life of native calpain-3 *in vitro* is less than 10 min, due to autolysis of the NS and IS1 regions (24). This makes purification of calpain-3 from skeletal muscle extremely difficult and is a barrier to studying the natural enzyme.

The NS sequence comprises ~50 residues that are rich in proline and glycine residues, thus implying an unstructured region (25). The 48-residue IS1 sequence is also largely

unstructured but with a short central region that is predicted to be alpha helix (26). The sequences and flanking sequences of NS and IS1 contain several proteolytic cleavage sites that are highly sensitive to exogenous proteases such as trypsin and chymotrypsin. IS1, however, is particularly prone to autoproteolysis (27) because it occupies the catalytic cleft of the protease core (28, 29) and the main autoproteolytic site is immediately adjacent to the active site cysteine. This suggests that IS1 functions as an internal propeptide to help regulate calpain-3 proteolytic activation (26, 28). By analogy to calpain-1, activation of calpain-3 occurs when two Ca<sup>2+</sup> occupy their conserved binding sites on either side of the protease core to cause a cooperative conformational change that forms the catalytic triad in the cleft (16). *In vitro* activation leads directly to autoproteolytic cleavage of IS1. However, when calpain-3 is anchored to titin in the sarcomere, it is conceivable that an effector molecule can pull IS1 out of the cleft (29). Alternatively, autoproteolysis of IS1 from the immobilized protease could happen without compromising the 3D structural

integrity of the enzyme core. While activated calpain-3 remains bound to titin, autolysis should remain intramolecular and be limited to IS1 cleavage. In this hypothetical model, damaged muscle proteins would be degraded *in situ* by the titin-bound protease.

The second insertion sequence, IS2, lies between the upstream CBSW domain and the downstream PEF domain. Deletion of the IS2 sequence increases both levels and stability of calpain-3 in the cytosol, suggesting that the IS2 sequence may also contain internal cleavage site(s) associated with the rapid degradation of calpain-3 (23). Further characterization of calpain-3 has demonstrated that the IS2 region can interact directly with the N2A and M-line regions of titin, a gigantic protein in myofibrils, implying that titin may be involved in regulating calpain-3 stability and activity (30–32) through IS2.

Unlike the conventional calpains-1 and calpain-2, calpain-3 is incapable of forming a heterodimer with the ubiquitously expressed calpain small subunit (21, 33). Biochemical and biophysical studies confirmed that recombinantly expressed PEF domain of calpain-3 forms a homodimer in strong preference to a heterodimer with the small subunit PEF domain (34). This was confirmed by the X-ray crystallography determination of the homodimerized PEF domain of calpain-3 (35). As expected, the fifth EF-hand motifs of the PEF domains are paired up, and there is a Ca<sup>2+</sup> in both of these motifs. Using size-exclusion chromatography, recombinant full-length inactive calpain-3 (C129S) eluted as a putative homodimer (33). More recently, an inactive calpain-3 expressed in COS7 cells has been reported by Hata *et al.* to form a homotrimer (36). In our attempts to produce recombinant calpain-3 for structural studies, we observed that the enzyme eluted from SEC at an apparent molecular weight larger than expected for a globular dimer. Our model for the dimer (35) indicated that the protein would be elongated and might have a larger apparent molecular weight because of its asymmetry.

To clarify calpain-3's oligomerization state and work towards an understanding of how LGMDR1 mutations affect the workings of the enzyme, we have used an *Escherichia coli* expression system to produce a stable recombinant inactive calpain-3 variant (C129A) with truncated NS and IS1 regions. Unexpectedly, this inactive full-length calpain-3 (C129A) ΔNS&IS1 largely exists as a homohexamer. Further analysis using single particle cryo-EM indicated that this protease forms a trimer of dimers and that the dimerization interaction is distinctly different from that seen in the crystal structure of the calpain-3 PEF domain homodimer. We also report that the homodimer is split into dimers upon binding to titin's N2A region and suggest that the oligomer is a way of sequestering calpain-3 until it can bind productively to the sarcomere.

## Results

### *In vitro* expression and purification of a stable recombinant human calpain-3 derivative

Characterization of endogenous calpain-3 has proven difficult because it undergoes rapid autoproteolysis during purification from muscle tissue extracts (33). One reason for

this is that IS1 occupies the active site cleft and is cut as soon as the enzyme is activated (27, 28). In previous experiments, where a large quantity of recombinant calpain-3 protease core was prepared for crystallography, the presence of NS and IS1 contributed to the core's susceptibility to both auto and endogenous proteolysis, while mutation of the catalytic cysteine residue 129 to serine still left a trace of protease activity (26, 28). Thus, to help ensure the stable production and purification of recombinant calpain-3 from *E. coli* in this study, we designed a calpain-3 construct—calpain-3 (C129A) ΔNS&IS1—in which NS and IS1 were deleted, and the active site Cys129 was mutated to Ala. After DEAE ion exchange chromatography, Ni-NTA affinity chromatography, and size-exclusion chromatography, approximately 0.35 mg of pure recombinant calpain-3 (C129A) ΔNS&IS1 was obtained per liter of culture. The stability of this purified calpain-3 was assessed by SDS-PAGE analysis of the enzyme stored in 100 mM NaCl, 20 mM Tris-HCl (pH 7.6), 2 mM EDTA, 10 mM 2-mercaptoethanol at 4 °C for up to 70 days. The 86-kDa protein migrated as a single protein band close to the 75-kDa molecular weight standard (Fig. S1). It is not known why the recombinant calpain electrophoresed ahead of where it should be, but this anomaly was consistently observed. The calpain-3 (C129A) ΔNS&IS1 derivative displayed significant stability under these Ca<sup>2+</sup>-free conditions, with no evidence of autolysis/proteolysis. Therefore, this storage condition was adopted in place of snap freezing and thawing aliquots.

### Recombinant calpain-3 is an oligomer in solution

Unlike calpains-1 and 2, calpain-3 is incapable of forming a heterodimer with the calpain small subunit (21, 33). However, the PEF domain of calpain-3 forms a stable homodimer in solution, which was confirmed by X-ray crystallography (35). Thus, the concept of homodimerization of calpain-3 was proposed and a dimer of the enzyme was modeled without any steric clashes, with an axis of symmetry running through the PEF domains, and with the two protease cores located at opposite ends of the dimer (34).

During the final step of calpain-3 (C129A) ΔNS&IS1 purification on size-exclusion chromatography in the presence of EDTA, the single peak of calpain-3 unexpectedly eluted close to where the ferritin molecular weight marker (474 kDa) chromatographed (Fig. 2A). The same result was obtained when the chromatography was repeated in the presence of Ca<sup>2+</sup>. This apparent molecular weight is more than 2.5 times larger than that expected for a homodimer of calpain-3 (C129A) ΔNS&IS1 (theoretical homodimer molecular weight 172 kDa).

Although the model for the calpain-3 dimer suggests that it is elongated in one direction, this asymmetry seems unlikely to explain such a large increase in apparent molecular weight. SDS-PAGE analysis of the SEC peak fractions showed a single protein band of ~75 kDa was present (Fig. 2B). To help characterize the calpain-3 oligomer, we

## Calpain-3 homohexamer dissociates to dimers on binding titin

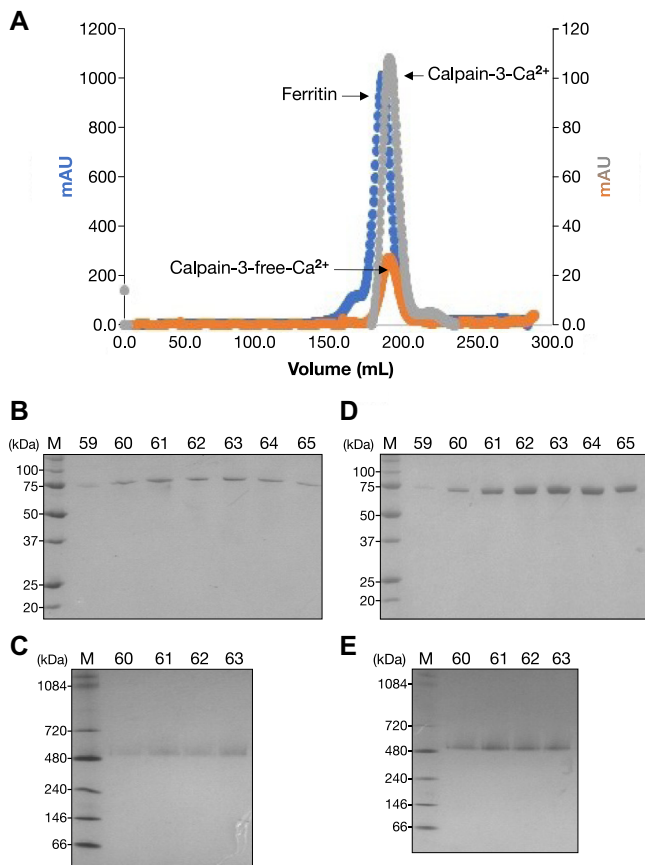


**Figure 2. Apparent molecular weight of calpain-3 (C129A)  $\Delta$ NS&IS1.** *A*, size-exclusion chromatography of calpain-3 and molecular weight markers on a HiLoad 26/60 Superdex 200 column. *Orange*:  $\text{Ca}^{2+}$ -free calpain-3 (right y-axis); *gray*: calpain-3 in the presence of 10 mM  $\text{CaCl}_2$  (right y-axis); *blue*: standard marker ferritin (left y-axis). *B* and *C*, calpain-3 peak samples in 2 mM EDTA separated on SDS-PAGE and BN-PAGE, respectively. *D* and *E*, calpain-3 peak samples in 10 mM  $\text{CaCl}_2$  separated on SDS-PAGE and BN-PAGE, respectively. Lane M shows the separation of molecular mass markers.

performed Blue Native PAGE (BN-PAGE) on freshly purified, unconcentrated samples of calpain-3 (C129A)  $\Delta$ NS&IS1. A single protein band was observed on the BN gels that migrated just slightly larger than the 480-kDa molecular weight marker (Fig. 2C).

To confirm the molecular weight of the calpain-3 oligomer by a method independent of its shape, the protein was assessed by multi-angle light scattering coupled with size-exclusion chromatography (SEC-MALS). Sodium azide and 2-mercaptoethanol were not added to the equilibration buffer for this chromatography to avoid these additive agents affecting the refraction index mismatch signal. The result indicated that 88% of the total mass fraction belonged to an oligomer of  $(479 \pm 0.1)$  kDa, which was consistent with the results of BN-PAGE. However, in addition, 7.2% of the total mass corresponded to a  $(1478 \pm 0.4)$  kDa species and 4.7% to a  $(4954.7 \pm 0.3)$  kDa species, respectively (Fig. 3A). These particles are three times and ten times larger, respectively, than the main peak material. It is possible that these smaller amounts of high molecular mass species in solution are a

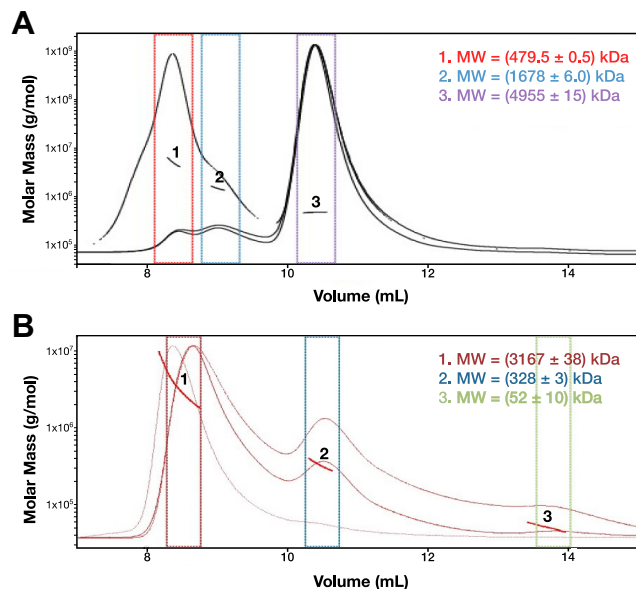


**Figure 3. SEC-MALS analysis of calpain-3 (C129A)  $\Delta$ NS&IS1 alone and in complex with titin-I81-I83.** *A*, elution of  $\text{Ca}^{2+}$ -free calpain-3 in the presence of 2 mM EDTA. Elution peaks are numbered in ascending molecular weight. *Lines* and *arcs* indicate peak molecular masses of calpain-3 in solution. *B*, elution of the calpain-3-titin-I81-I83 complex in the absence of  $\text{Ca}^{2+}$ . *Lines* and *arcs* indicate peak molecular masses of calpain-3 and titin-I81-I83 in solution.

result of artifactual sample aggregation during the experiment and may not occur naturally.

The results of SEC, BN-PAGE, and SEC-MALS indicate that calpain-3 (C129A)  $\Delta$ NS&IS1 forms an oligomer potentially ranging from a pentamer ( $\sim 430$  kDa) to a hexamer ( $\sim 516$  kDa). However, since PEF domains are invariably paired up (37), it seems most likely that the oligomer is a hexamer. Because macromolecule mass in solution can be affected by many factors, such as protein concentration, shape, and buffer solutions, we explored three other biophysical methods of probing the oligomeric status of this inactive calpain-3 multimer.

### Calpain-3 sediments as an oligomer in the size range of a pentamer to a hexamer

The comparison of high and low concentration samples of calpain-3 clearly showed reversible self-association (Fig. 4A, blue and green lines), as can be inferred from the right-shift of the sedimentation profiles. At low concentration (Fig. 4A, blue line), about 13% of the total concentration at 1.84 S is consistent with a monomeric species. At higher concentration (Fig. 4A, green line), a stable 14 S species is formed ( $\sim 75\%$  of the total concentration), with a slight tendency to oligomerize further into species with values between 15 and 30 S. When the low concentration sample is subjected to cross-linking (Fig. 4A, red line), the same 14 S species is evident, though at a lower concentration ( $\sim 45\%$  of the total concentration). In addition, much larger aggregates were observed as a result of cross-linking. Both the high concentration sample and the cross-linked sample were also fitted by a parametrically

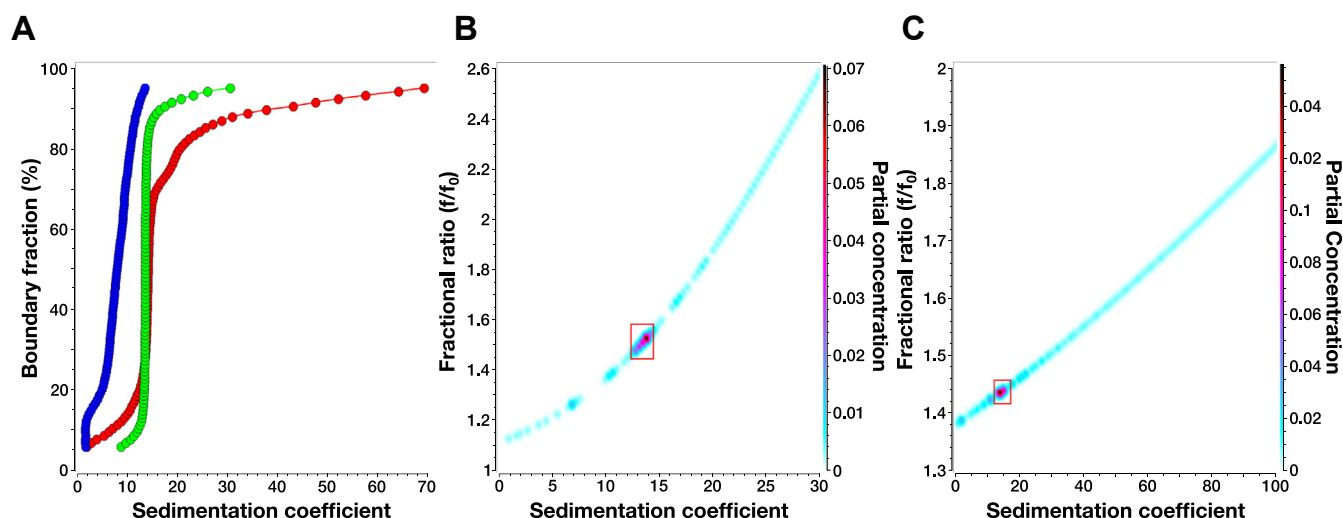


**Figure 4. Sedimentation velocity analysis of calpain-3 (C129A)  $\Delta$ NS&IS1.** A, model-independent integral sedimentation coefficient distributions from an enhanced van Holde–Weischet analysis of calpain-3 (blue: 0.3  $\mu$ M, green: 1.75  $\mu$ M, red: 0.3  $\mu$ M, cross-linked). Reversible self-association is clearly evident from the right-shift of the green (high concentration) profile compared to the blue (low concentration) profile. A stable species around 14 S is apparent at high concentration ( $\sim$ 75% of total concentration) and at low concentration ( $\sim$ 45% of total concentration) when cross-linking was employed. B, PCSA-Monte Carlo analysis of calpain-3 at high concentration (green line in A). A major species is observed around 14 S. Integration results from the indicated red square are presented in Table 1. C, PCSA-Monte Carlo analysis of cross-linked calpain-3 at low concentration (red line in A). A major species is observed around 14 S; integration results from the indicated red square are presented in Table 1.

constrained spectrum analysis-Monte Carlo analysis to determine molecular parameters for the stable oligomeric form (Fig. 4, B and C). The molecular parameters are listed in Table 1. The results suggest that the oligomerization of calpain-3 forms increasingly nonglobular species as mass increases. The stable 14 S species has an elevated nonglobular frictional ratio of  $\sim$ 1.4, suggesting a slightly nonspherical shape of the assembly. The molar masses estimated from the molecular parameters for the stable species are consistent with either a pentameric or hexameric oligomer for calpain-3.

#### Solution structure analysis by small angle X-ray scattering indicates calpain-3 forms a homohexamer

The fact that calpain-3 forms an oligomer in solution has been confirmed by the previous biophysical experiments. However, oligomeric masses showed some variation from experiment to experiment. Thus, the calpain-3 oligomer’s assembly and shape in solution may affect molecular mass determination. To probe the molecular envelope of the calpain-3 oligomer in solution, small angle X-ray light scattering (SAXS) experiments were conducted. The effect of protein concentration on the modular structure was compared by collecting SAXS data using calpain-3 samples at 1.5 mg/ml

and 3.0 mg/ml. The scattering patterns of both samples were similar (Fig. 5A). The scattering patterns in the low q region of the respective Guinier plots, as well as the values of  $R_g$  and  $I(0)$  that were calculated by PRIMUS (38) and GNOM (39), were in agreement for both concentrations of the sample, thus indicating no signs of aggregation or intermolecular repulsion in either sample (Table 2).

The pair distance distribution function  $P(r)$  was calculated with GNOM. Estimated maximum dimension ( $D_{max}$ ) values of 158.6 Å and 163.4 Å were obtained for the 1.5 mg/ml and 3 mg/ml samples, respectively, from the SAXS data sets. Comparison of the  $P(r)$  functions calculated from experimental scattering by GNOM (39) from both samples showed characteristic bell-shaped curves (Fig. 5B), indicating that the protein folds into a globular shape in solution. These bell-shaped curves were identical to the bell-shaped Kratky plots (Fig. 5C). Using the Shape&Size calculation of molecular mass in the ATSAS suite (40), the result shows masses of 432 kDa for the 1.5 mg/ml sample and 435 kDa for the 3 mg/ml sample, respectively (Table 3). Both mass values agree with those obtained here by SEC and SV-AUC.

*Ab initio* shape reconstruction of the SAXS data was carried out in DAMMIN (41) from which a set of ten models were

**Table 1**  
Molecular parameters for the stable species found in calpain-3 high concentration and cross-linked (XL) sample

Sample analysis method	Sedimentation coefficient (95% conf. interval)	Estimated molar mass (Da) (95% conf. interval)	Partial concentration	Fractional ratio $f/f_0$
1.75 $\mu$ M, PCSA	13.6 S (11.8 S–15.3 S)	429,100 (311,500–546,800)	73.60%	1.51
0.3 $\mu$ M XL, PCSA	14.4 S (12.2 S–16.6 S)	429,100 (311,500–546,800)	43.70%	1.44
1.75 $\mu$ M, vHW	$\sim$ 14 S		$\sim$ 75%	n/a
0.3 $\mu$ M XL, vHW	$\sim$ 14 S		$\sim$ 45%	n/a

## Calpain-3 homohexamer dissociates to dimers on binding titin

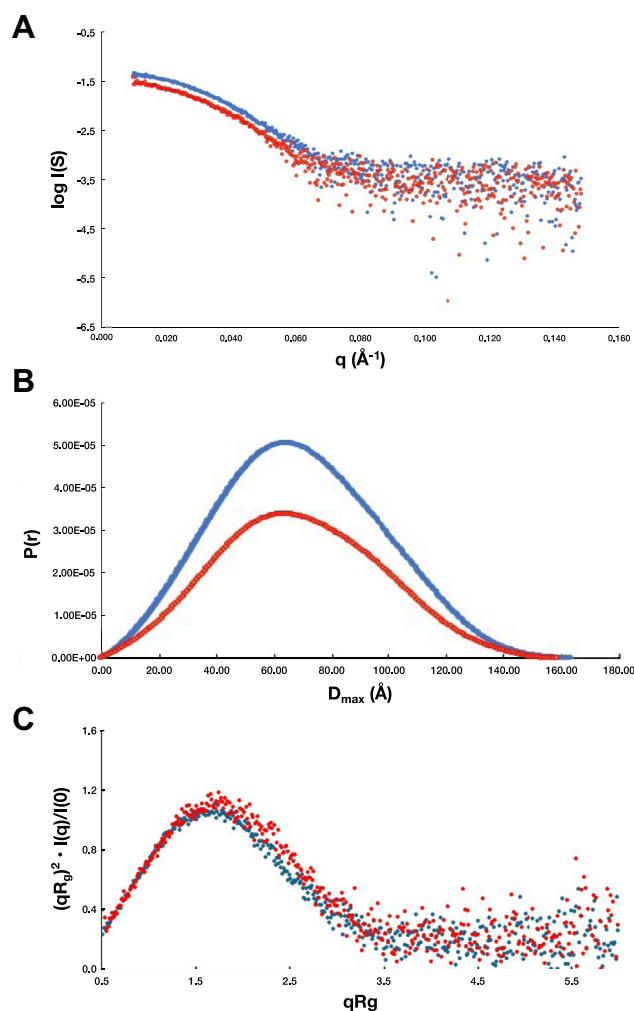


**Figure 5. Small-angle X-ray scattering analysis of calpain-3 (C129A)  $\Delta$ NS $\Delta$ IS1 in solution.** A, superposition of scattering curves from the 3.0 mg/ml calpain sample (blue) and the 1.5 mg/ml sample (red). B, distance distribution function measurement are from 3.0 mg/ml (blue) and 1.5 mg/ml (red) samples. C, Kratky plot shows protein folding. Blue and red correspond to the 3.0 mg/ml and 1.5 mg/ml samples, respectively.

superimposed and averaged by DAMAVER (40). The normalized spatial discrepancy values of the models were very similar, with mean values of  $0.521 \pm 0.015$  and  $0.534 \pm 0.029$ , corresponding to the 1.5 mg/ml and 3 mg/ml samples, respectively. The shape of the modeled structure envelope resembled an irregular ellipse profile (Fig. 6A). In order to determine the oligomer form this *ab initio* shape reconstructed model of SAXS corresponds to, we used AlphaFold2 (42) to predict a structural model of calpain-3 lacking NS and IS1 and generated a homodimer mimicking the dimer crystal structure of the calpain-3 PEF domain (PDB ID: 4OKH) by aligning the two complementary unpaired fifth EF-helix motifs

of PEF-hand domains from two calpain-3 structures (Fig. 7). This homodimerization module again placed the two protease cores at either end of the model (Fig. 7A) with their unstructured IS2 regions protruding externally (Fig. 7, B and C).

Subsequent energy minimization and molecular dynamics simulations showed no obvious steric barriers for calpain-3 homodimerization. Two homodimers of calpain-3 were fitted into the *ab initio* reconstructed envelope. Subsequently, three calpain-3 homodimers without IS2 were readily fitted into the *ab initio* reconstructed envelope. CRYSOLOG (43) was used to evaluate the fit of the solution scattering data from calpain-3 (C129A)  $\Delta$ NS $\Delta$ IS1 organized as three-homodimer structures. The result reveals the hexamer structural model of calpain-3 is in good agreement with the experimental scattering data and produced a  $\chi^2$  value of 0.97 (Fig. 6B).

### Three dimers of calpain-3 are present in the single particle cryo-EM map

To verify calpain-3 forms a hexamer, to obtain an atomic model, and to examine the interface connections within the oligomer, we conducted a single particle cryo-EM analysis. The data for 4,029,390 particles of calpain-3 were collected from 4888 micrographs (Fig. S2A). After two-dimensional (2D) classification, the better 2D classes from 596,621 particles (Fig. S2B) were subjected to 3D *ab initio* reconstruction and 3D classification. Particles in the best class (334,733 particles) were selected and used for 3D map refinement with  $D_3$  symmetry. As a result, the calpain-3 refined map was determined at an overall FSC<sub>0.143</sub> of 3.85 Å.

The 3D reconstruction map revealed how calpain-3 forms oligomers. The middle region of the map where the six PEF domains come together is a relatively rigid region, in which the local resolution reaches 2.9 Å (Figs. 7A and S3). However, the peripheral regions of the map where the six protease cores are located appear quite flexible with a much lower resolution than overall (Fig. 7B). The outline architecture of the calpain-3 map shows a “three-leaf clover” shape in the middle region (colored dark blue on the resolution scale) and six angular protrusions around the “three-leaf clover” center with resolution  $\sim 6$  Å (Fig. 7, A and B). On closer inspection, after rendering the map at a higher density level in UCSF Chimera (44), we found a four-helix-bundle density organized as a repeated element with a total of three of these repeats present in the density (Fig. 8, A and B). Each four-helix bundle has an axis of symmetry suggestive of an interface between dimer pairs (colored orange and green). By fitting helices from the calpain-3 PEF domains to these densities, we were able to recognize the four-helix bundle as being composed of the last two helices of the C-terminal PEF domains from a calpain-3

**Table 2**  
BioSAXS statistics summary of calpain-3 (C129A)  $\Delta$ NS $\Delta$ IS1

Sample: Calpain-3	Guinier			GNOM				Shape&Size
	Rg	I(0)	qRg	Rg	I(0)	Quality (%)	Dmax (Å)	MM (kDa)
1.5 mg	55.6 $\pm$ 1.3	0.03 $\pm$ 0.0006	1.29	53.0 $\pm$ 0.5	0.03 $\pm$ 0.0003	97	158.6	431.59
3.0 mg	51.9 $\pm$ 0.7	0.05 $\pm$ 0.0005	1.3	53.1 $\pm$ 0.3	0.05 $\pm$ 0.0003	92	163.4	435.27

**Table 3**  
BioSAXS data collection and analysis

Dataset	Calpain-3 data-1	Calpain-3 data-2
Beamline	ID7A1	ID7A1
Wavelength range (Å)	1.264828	1.264828
q range (Å <sup>-1</sup> )	0.005-0.7	0.005-0.7
Exposure time per frame (s)	2	2
Measured method	SEC-SAXS	SEC-SAXS
Measured concentrations (mg/ml)	1.5	3
Temperature (K)	278	278
Structural parameters for averaged data		
I(0) (from Guinier analysis)	0.033 ± 0.00057	0.047 ± 0.00048
R <sub>g</sub> (Å) (from Guinier analysis)	55.64 ± 1.26	51.89 ± 0.71
I(0) (from P(r))	0.032 ± 0.00032	0.047 ± 0.00031
R <sub>g</sub> (Å) (from P(r))	52.92 ± 0.50	53.11 ± 0.29
D <sub>max</sub> (Å)	158.63	163.4
Shape&Size molecular mass (kDa)	431.59	435.27
Monomer molecular mass from sequence (kDa)	85.684	85.684
Software employed		
Primary data reduction	BioXTAS RAW	BioXTAS RAW
Data processing	RAW series analysis ATSAS	RAW series analysis ATSAS
<i>Ab initio</i> analysis	DAMMIN	DAMMIN
Validation and averaging	DAMAVER	DAMAVER
Evaluation scattering from atomic structure	CRYSOL	CRYSOL

dimer. This confirmed the central location of the PEF domains as indicated in Figure 7A.

By rendering the map at a lower density level, we observed how the six subunits of calpain-3 are assembled and occupy the EM-density map (Fig. 9, A–C). The yellow core of the oligomer seen in Figure 9A is occupied by the three PEF dimers from which emanate six calpain beta-sandwich domains (pink) connected to the protease core domains PC1 and PC2, colored blue and green, respectively. These peripheral domains make up the six angular protrusions seen in Figure 7B coming from the core trimer of PEF dimers. When this view is horizontally rotated by 90°, the central red coloration of yellow highlights a PEF dimer interface (Fig. 9B). Two protease cores are seen on the top of the figure and two at the bottom, with the other two being hidden from view on the other side of the oligomer. The third view in this figure hints at a close association between pairs of protease core domains (Fig. 9C). Although we presently do not have sufficiently high resolution in this part of the map to be confident of the details of their interaction, we do have the crystal structure of the protease core to work from (28).

We can, however, be sure that the calpain-3 hexamer is built around the three-way association between PEF dimers at the core of the oligomer that imparts the 3-fold axis of symmetry (Fig. 10, A and B). Here the PEF dimer pairs are colored green and red, gray and mauve, and blue and yellow. The three PEF dimer interfaces (Fig. 10C) are centered on the four-bundle helical density elements in the middle region of the map featured in Figure 8. In the entire density map, all three of these monomer–monomer interfaces can be seen and are identical. A close-up of the homodimer interface in the cryo-EM structure reveals many hydrophobic interactions between the four contacting helices (Fig. 10D) that can account for the tight binding through this interface. We also found several contacts between PEF domains that account for the ability of the PEF dimers to trimerize. These contacts come

from helix4 on one PEF domain dimer and helix6 from a neighboring dimer PEF domain along with several hydrophobic and electrostatic contacts to further help hold the three dimers together. These trimerization contacts are between the green and gray, mauve and blue, and red and yellow-colored PEF domains (Fig. 10A).

#### PEF domain dimerization surfaces are different between solution and crystal structures

With these three interfaces mapped out, we attempted rigid body fitting of the PEF domain to this density region. We tested fitting the crystal structure of calpain-3 PEF domain (PDB ID: 4OKH), calpain-2 PEF large subunit (PDB ID: IDFO), which is a homolog of calpain-3 with 47.6% sequence identity, and the AlphaFold-predicted calpain-3 PEF domain, but all these trials failed due to a large mismatch. Next, we used a ‘dissect-and-build’ approach from the crystal structure of calpain-3 PEF domain (PDB ID: 4OKH) along with the assistance of a raw structure path in the density map that was created by ModelAngelo (45). In this way, all six PEF domains of calpain-3 were manually built into the middle density of the EM map. What is surprising and could not have been predicted is that all three PEF homodimer association interfaces are the same as the one shown in Figure 11A and are substantially different from those seen in the crystal structure of the calpain-3 PEF domain dimer (Fig. 11B) (35) as well as in the calpain-2 heterodimer crystal structure (Fig. 11C) (19, 20) and in the crystal structure of the small subunit PEF domain homodimer (Fig. 11D) (17, 18).

#### Binding of titin to calpain-3 splits the oligomer into dimers

Calpain-3’s association with select regions of the muscle protein titin is thought to be the key to its function of muscle protein turnover after eccentric exercise (46). Major binding sites on titin for the enzyme have been identified as two

## Calpain-3 homohexamer dissociates to dimers on binding titin

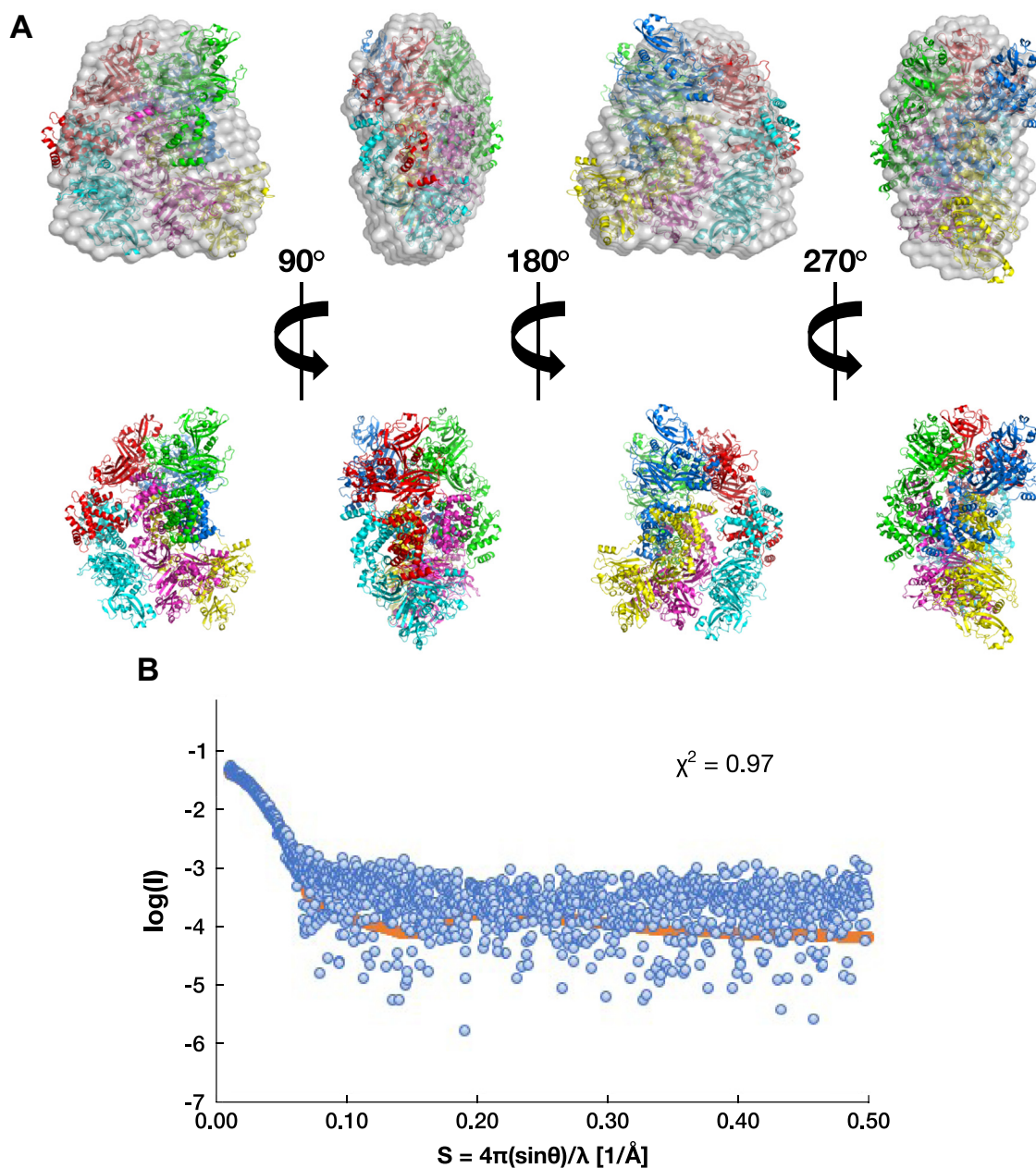


**Figure 6. Fitting of the calpain-3 solution scattering data to the homohexamer structure model.** A, AlphaFold2-predicted three homodimer structures of calpain-3 lacking insertion sequences are shown fitted into the *ab initio* model envelope of calpain-3 solution experimental scattering from four different view angles. In the second row, the structures without the envelope colored red, marine blue, green, yellow, cyan, and magenta represent six individual calpain-3 molecules. B, CRYSOLE fitting plot shows experimental scattering of calpain-3 (blue spheres) in relations to the homohexamer structure model of calpain-3 (red line).

distinct regions, the N2A and M-lines, respectively (30, 32). However, it is not known if calpain-3 binds there as a monomer, dimer, or oligomer. The binding site on the enzyme has been identified as the IS2 sequence that projects between the calpain beta-sandwich domain and the PEF domain (Fig. 7). This region was left in the calpain-3 construct from which NS and IS1 had been removed to have the option of studying calpain-3's binding to titin. The titin fragment alone was abundantly expressed in *E. coli* and easily purified as demonstrated for a slightly shorter version by Stronczek *et al.* (47). For those reasons, when the titin construct was co-expressed

with calpain-3, it was placed in a low copy number plasmid to better balance the yields of the two products.

After purification of the recombinant products, there was a decrease in the molecular weight of the main protein band from 480 kDa to 320 kDa when electrophoresed on a Blue Native gel, and some unbound titin appeared to be carried along in the purification of the complex while some hexamer remained at 480 kDa (Fig. 12A). To examine the composition of the 320-kDa product, a lane of the Blue Native gel was soaked in SDS and its proteins were analyzed in a second dimension by SDS-PAGE (Fig. 12B). The two-

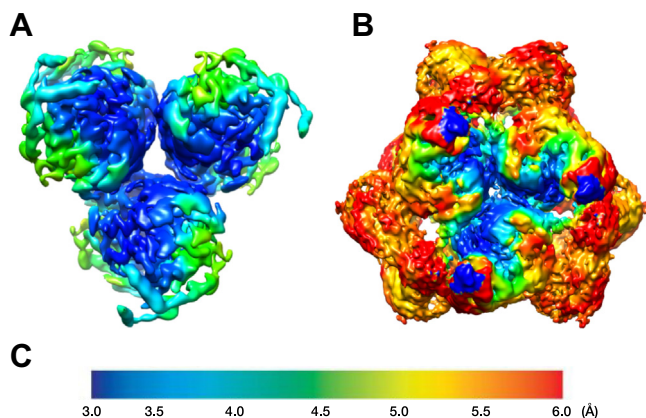


**Figure 7. Refined cryo-EM map.** A, calpain-3 segmented core map showing the 3-fold  $D_3$  symmetry of the PEF domains at contour level 0.2. B, overall calpain-3 reconstruction map showing the more flexible protease core domains on the periphery of the map. C, scale of resolution from dark blue (3 Å) to red (6 Å).

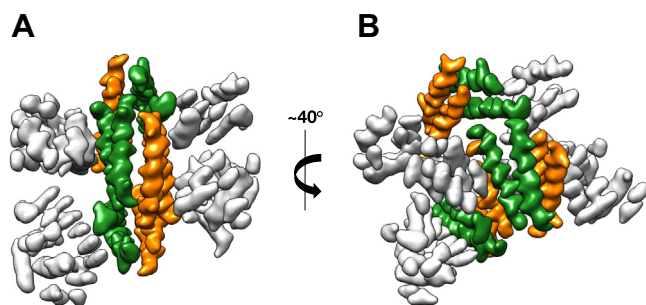


**Figure 8. Calpain-3 PEF domain segmentation.** The four-helix helical bundle in the central core is represented at a contour level of 0.67. Two views (A and B) are shown rotated by  $40^\circ$  to each other. Green and orange represent the paired helices from the two different PEF domains that are the dimerization interface.

dimensional gel showed that the 320-kDa band was composed of calpain-3 and titin in a roughly 1:2 stoichiometry to give a combined molecular weight of  $2 \times 86 \text{ kDa} + 4 \times 37 \text{ kDa} = 320 \text{ kDa}$ .

Interestingly, whether calpain-3 was co-expressed and copurified with titin N2A region I81-I83 fragment or both proteins expressed and purified individually and then incubated together, we found that they formed a complex (Fig. 12, B and C). However, the molecular mass of this complex was much less than that of calpain-3 alone in solution. This complex showed the molecular mass was  $\sim 320 \text{ kDa}$  from the SEC-MALS second peak (Fig. 3B) and BN-PAGE (Fig. 12A). In SEC-MALS, the first peak molecular mass was  $(3167 \pm 38) \text{ kDa}$ , which suggested the sample had some aggregation during the experiment, and the third peak molecular mass was  $(52 \pm 10) \text{ kDa}$ , which indicated some unbound free titin-I81-I83 in the copurified sample that was consistent with the two-dimension gel (Fig. 12B) showing some unbound titin-I81-I83. To avoid sample degradation, we also checked the time-course experiment. The results did not show any degradation occurred during more than 2 months of observation (Fig. S4). Based on the molecular mass calculation, the

monomer of calpain-3 (C129A)  $\Delta\text{N}\&\text{IS1}$  is  $\sim 85.7 \text{ kDa}$  and the monomer of titin N2A region I81-I83 fragment is  $\sim 37.5 \text{ kDa}$ . If a monomer calpain-3 binds two titin-I81-I83 fragments, the mass ratio of calpain-3 to titin would be  $\sim 1:2$ . Therefore, the doubled molecular masses at 1:2 stoichiometry ( $\sim 320 \text{ kDa}$ ) is a good agreement with the results of SEC-MALS and BN-PAGE. That implies a calpain-3 dimer binds four titin-I81-I83 molecules.

## Discussion

PEF domain proteins are always found in pairs (37) with the fifth EF-hand motif serving as the dimerization interface (48). As described above, this observation has been borne out in the human calpain family where about half of the members possess a PEF domain at their C-terminus. Calpain crystal structures have documented examples of both homodimerization and heterodimerization through PEF domains. For calpain-3, its PEF domain expressed as a recombinant protein in *E. coli* forms a strong dimer by pairing of the fifth EF-hand (35). During the characterization of the recombinant calpain-3 oligomer by the various biophysical techniques used here, the primacy of the PEF pairing led us to discount suggestions that the oligomer might be a pentamer or a heptamer. Although the weight of evidence was in favor of the oligomer being a hexamer, it was reassuring to see this unequivocally established by the cryo-EM structure that showed the calpain-3 complex was a trimer of dimers.

During the early stages of this study, Hata *et al.* (36) reported that the 94-kDa calpain-3 (C129S) recombinantly expressed in COS7 cells or extracted from skeletal muscle of knock-in mice had mobility on BN-PAGE consistent with a mass greater than 240 kDa that most closely resembles a trimer theoretical molecular weight of 282 kDa. Cross-linking with glutaraldehyde prior to biophysical analysis gave similar results suggesting that this trimer-sized particle was not a breakdown product of a larger assembly. These authors reported that the calpain-3 PEF domain was needed for trimer formation but when it was expressed as an isolated domain, it formed a homodimer, consistent with our observations (35). They also showed that the removal of the insertion sequences IS1 and IS2 from calpain-3 still produced a trimer. The most puzzling aspect of these results is the suggestion that a PEF domain remains unpaired. This conundrum could likely be resolved by the use of single particle cryo-EM given that the complex is large enough at  $\sim 280 \text{ kDa}$  for this methodology to be used and for the results to be compared with those from this study.

Ironically and surprisingly, after relying heavily upon the fifth EF-hand pairing to argue for a fundamental underlying dimer, the cryo-EM structure shows that this is not the motif pairing that dimerizes the PEF domains within the oligomer. Instead, it is the formation of a four-helix-bundle structure involving helices from EF-hands 4 and 5 that joins the calpain-3 dimers together in all three instances in the hexamer. In the early days of calpain structural biology, an attempt was made to render the calpain small subunit PEF

## Calpain-3 homohexamer dissociates to dimers on binding titin

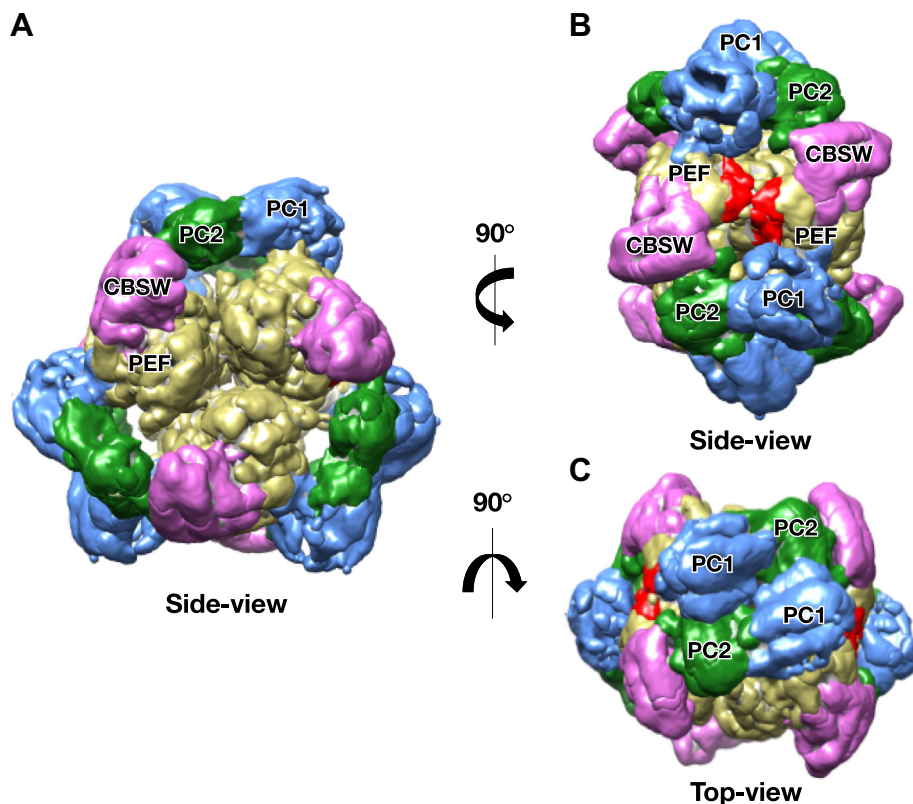


**Figure 9. Delineation of six calpain-3 molecules in the cryo-EM density map of the hexamer showing their subdomains in different colors at a threshold level of 0.12.** A, side view showing protease core domain PC1 in blue; protease core domain PC2 in green; the calpain-3 beta-sandwich domain in pink; and the PEF domain in yellow. B, 90-degree vertical rotation from the view in (A) where red represents the interface between two PEF domains of a calpain-3 dimer. C, 90-degree horizontal rotation from (A).

domain monomeric by removing its fifth EF-hand (49). After this deletion, an asymmetrical dimer formed in place of two monomers indicating that this domain has more than one surface available for protein–protein interactions. It would be interesting to know which of the two PEF interactions is the lower energy state. In our working hypothesis for the role of the calpain-3 hexamer in functioning human muscle, we envisage oligomerization as a way of sequestering an autoproteolytically active enzyme from the point of synthesis on polysomes to its deposition into the N2A region of aligned titin molecules in the sarcomere (Fig. 13). When the hexamer dissociates there, do calpain-3 dimers form through the fifth EF-hand pairing at a lower energy state to help drive this reorganization? This could occur in conjunction with a positive association from the IS2 region of calpain-3 binding to titin. If so, preventing a preferred dimer association through the fifth EF-hands from forming too early might be a way of spring-loading the oligomer to dissociate under the right conditions provided by titin in the sarcomere.

Beyond the dimerization issue is the question of how the dimers come together to form the hexamer. Within the core of the hexamer, the three PEF-dimers pack together through surface associations of helices 4 and 6. Each dimer pair projects in the opposite direction and the role of the beta-sandwich domain seems confined to being

the linkage to the protease core region. Looking at the protease core regions on the outer surface of the hexamer, there is an intimate pairing of PC1 and PC2 from one core with the PC1 and PC2 domains from a neighboring core that belongs to a different dimer in the hexamer (Fig. 9). This association has two axes of symmetry, one running through the PC1 pair and one through the PC2 pair. Unfortunately, these three examples of core dimerization lie on the outer edge of the oligomer where the resolution is insufficient to delineate specific residues in binding. Crosslinking studies could potentially be used to confirm the juxtaposition of neighboring residues and their distance apart in the oligomer.

In designing the more proteolytically resistant calpain-3 (C129A)  $\Delta$ NS&IS1 for the oligomerization study, the intrinsically disordered IS2 region was left in the construct at the risk of increasing proteolysis because it was expected to be the landing pad for titin. Co-expression studies with the select titin fragment have validated this strategy by showing that the calpain-3 oligomer undergoes a remarkable breakdown into titin-bound dimers. Finding out the mechanism behind this transition is an important future direction of inquiry. However, the flexibility of the titin-bound calpain-3 dimer does not lend itself well to cryo-EM single particle analysis. Nevertheless, crystallography of select regions of the dimer complex with titin might reveal, for example, if the PEF dimerization

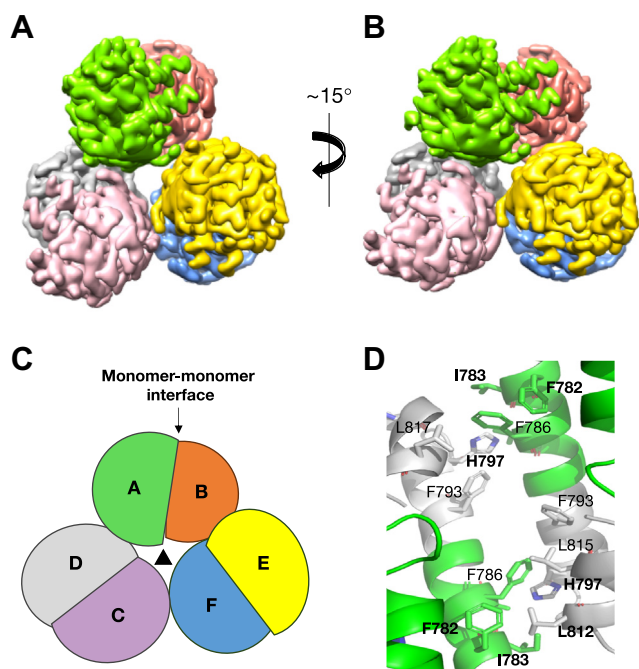


**Figure 10.** Close-up view of the six PEF domains that comprise the hexamer core. A and B, cryo-EM density map of the calpain-3 hexamer core showing its 3-fold symmetry axis at a contour level of 0.4 with two different perspectives rotated 15° to each other. The PEF domains from the six subunits are shown in different colors: green, orange, purple, gray, yellow, and blue. C, schematic of the monomer-monomer interfaces represented in (A and B). D, close-up view of the hydrophobic residues involved in the dimerization interface between two PEF domains of calpain-3. The bold-residues represent mutated residues (<https://www.dmd.nl/>) that cause LGMDR1.

has switched to the fifth EF-hand pairing during the dissociation.

Another pressing area for further examination is the mapping of surface LGMDR1 point mutations onto the hexamer to see if any of them might destabilize the oligomer. Previously, we would have focussed on the fifth EF-hand region. But now, it is clear that the dimerization region in the oligomer includes nearby helices and that the PEF trimerization interface includes other PEF domain surfaces. At the other end of the oligomer, it will be necessary to interpret surface mutations in the protease core domains to see if any might make contacts between the cores. Some candidate LGMDR1 mutations at the dimer and trimer interfaces are listed in Table S2. Not only should these mutations be mapped but they should be reproduced in the calpain-3 (C129A) ΔNS&IS1 construct to see if they weaken or block the assembly of the hexamer.

## Experimental procedures

### Cloning and expression of recombinant calpain-3

To avoid rapid proteolysis of recombinant calpain-3 produced in *E. coli*, a construct was made from which 45 residues of NS (P<sup>2</sup> – I<sup>46</sup>) and 48 residues of IS1 (D<sup>268</sup>GTNM—RPTR<sup>315</sup>) were deleted. In addition, the catalytic cysteine of the active site (Cys129) was changed to Ala129 to eliminate autoproteolytic activity. Human calpain-3 isoform\_1 (NM\_000070.3) was used as a template from which GeneArt

(Thermo Fisher Scientific) synthesized the modified gene following codon optimization. The synthesized DNA was inserted into a pET24a vector such that the expressed product would have a C-terminal hexa-histidine tag under kanamycin selection. Positive clones were verified by DNA sequencing and transformed into the BL21PLySs (DE3) strain of *E. coli*. For the co-expression of calpain-3 with titin-I81-I83, the human titin N2A region Ig81 to 83 fragment gene (NM\_133378.4) was codon optimized by GeneArt, and the synthetic DNA sequence was inserted in a pACpET vector (50) to produce the protein without a His-tag under ampicillin selection. The positive clones were verified by DNA sequencing, and then the plasmids of titin I81-I83 and calpain-3 C129A ΔNS&IS1 were transformed into *E. coli* strain BL21(DE3) for protein expression under kanamycin and ampicillin selection.

A single clone was picked and inoculated into LB media (3 ml) containing antibiotic (0.05 mg/ml kanamycin for calpain-3 alone and 0.05 mg/ml of kanamycin plus 0.1 mg/ml of ampicillin for the calpain-3/titin complex) and incubated with shaking (220 rpm) for 8 h at 37 °C. This 3-mL culture was then added into 200 ml of LB media containing antibiotic and allowed to grow overnight at 37 °C with shaking (220 rpm). Subsequently, the overnight 200-mL culture was used to inoculate eight 1-L cultures grown under the same conditions until their A<sub>600</sub> reached 1.0, at which point protein expression was induced by the addition of isopropyl β-D-1-thiogalactopyranoside to a final concentration of 0.4 mM. After additional culturing for 16 h at 20 °C, cells were harvested by centrifugation.

### Purification of recombinant calpain-3

Calpain-3 and calpain-3–titin-I81-I83 complex were purified from lysed *E. coli* using protocols developed for calpain-2 isolation (51) with some modifications. Briefly, cells were lysed by sonication in buffer A [50 mM Tris–HCl (pH 7.6), 5.0 mM EDTA, 10 mM 2-mercaptoethanol] containing one tablet of protease inhibitor cocktail (Roche), which can inhibit a broad spectrum of serine and cysteine proteases, and the cell debris were removed through centrifugation at 48,000g for 60 min. The supernatant was applied to a DEAE ion-exchange column that had been pre-equilibrated with buffer A. After washing away unbound material, calpain-3 was eluted from the column using a gradient of 0 to 0.75 M NaCl in buffer A. Fractions containing calpain-3 based on SDS-PAGE analysis were combined and MgCl<sub>2</sub> was added with gentle stirring to a final concentration of 23 mM in order to saturate the 5 mM EDTA and avoid stripping Ni<sup>2+</sup> from the Ni-NTA resin used in the next purification step. The sample was applied to a Ni-NTA column, washed with 50 mM Tris–HCl (pH 7.6), 100 mM NaCl, and 5 mM imidazole, and eluted wash buffer supplemented with 250 mM imidazole. Elution fractions containing calpain-3 according to SDS-PAGE were dialyzed into a buffer containing 20 mM Tris–HCl (pH 7.6), 100 mM NaCl, 2 mM EDTA, 10 mM 2-mercaptoethanol, 0.05% sodium azide, and two tablets of protease inhibitor cocktail. Lastly, the calpain-3–

## Calpain-3 homohexamer dissociates to dimers on binding titin

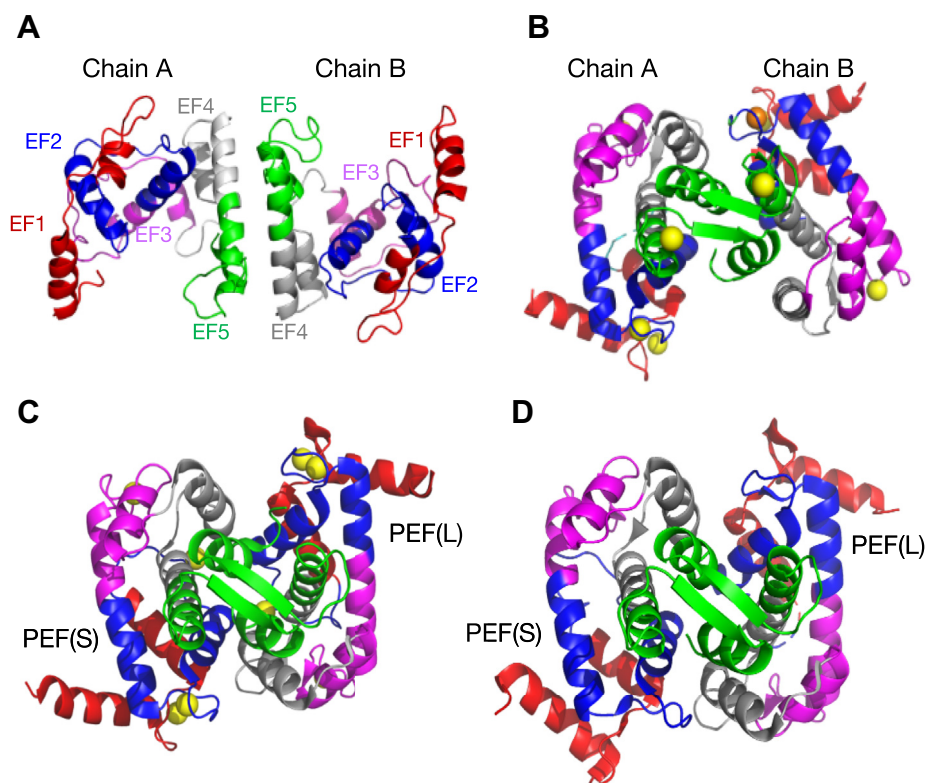


**Figure 11. Comparison of calpain-3 PEF structures association from homodimer and calpain-2 PEF(L) and PEF(S) association from heterodimer structure in ribbon diagram format.** A, calpain-3 PEF domain homodimerization solved by single particle cryo-EM; B, calpain-3 PEF domain interactions revealed by the crystal structure in the presence of calcium (PDB ID: 4OKH); C, PEF domain interactions between calpain-2 large subunit and the small subunit with calcium present as shown by the crystal structure (PDB ID: 3BOW); D, PEF domain interactions between calpain-2 large subunit and the small subunit in the absence of calcium as shown by the crystal structure (PDB ID: 1DF0). Structures are shown in ribbon format with different colors representing the five EF-hand helical motifs as delineated in (A).

enriched sample was applied to a Superdex 200 column (Amersham Biosciences) for a final purification step. Protein purity was assessed using SDS-PAGE visualized by Coomassie Blue. All purification procedures were performed at 4 °C.

### Proteolysis assay

The susceptibility of calpain-3 (C129A) $\Delta$ NS&IS1 and calpain-3–titin-I81-I83 preparations to proteolysis over time was assessed in the absence of  $\text{Ca}^{2+}$  using SDS-PAGE. Protein was assayed in 20 mM Tris–HCl (pH 7.6), 100 mM NaCl, 2 mM EDTA, and 10 mM 2-mercaptoethanol. Samples were stored at 4 °C in a final volume of 400  $\mu$ l with a protein concentration of 0.5 mg/ml. Aliquots were removed at time points ranging from 0 to 70 days and the reaction was stopped by the addition of 3X SDS-PAGE loading buffer followed by heating at 95 °C. The samples were analyzed by SDS-PAGE with the protein bands visualized by Coomassie Blue staining.

### Molecular mass estimation by size-exclusion chromatography

A size-exclusion chromatography column (HiLoad 26/60 Superdex 200) was equilibrated with 20 mM Tris–HCl (pH 7.6), 100 mM NaCl, 2 mM EDTA, 10 mM 2-mercaptoethanol, and 0.05% sodium azide at 4 °C. The column was then calibrated with molecular weight standards listed in Table S1.

Following calibration, calpain-3 (C129A) $\Delta$ NS&IS1 was loaded onto the column. Protein was detected in the eluate by measuring the absorbance of fractions at 280 nm and analyzing 'peak' fractions by SDS-PAGE.

### Multi-angle light scattering coupled with size-exclusion chromatography

Multi-angle light scattering experiments were performed at the University of Toronto. For SEC-MALS, protein samples were chromatographed on a Superdex 200 Increase 10/300 column coupled to a Wyatt multi-angle light scattering analyzer with dynamic light scatter and refraction index detectors in-line to an ÅKTA Pure FPLC at 4 °C. The system was pre-equilibrated using running buffer (20 mM Tris–HCl pH 7.6, 100 mM NaCl, and 2 mM EDTA) overnight. A fresh solution of bovine serum albumin (1 mg/ml) was prepared using the same running buffer for system calibration as well as 5 mg/ml of either calpain-3 (C129A) $\Delta$ NS&IS1 or calpain-3 (C129A) $\Delta$ NS&IS1/titin-I81-I83. Aliquots (100  $\mu$ l) were loaded onto the column. The running buffer was prepared in the absence of a reducing agent and sodium azide in order to avoid any refraction index mismatch signal. The column was run at a flow rate of 0.4 ml/min with a maximum pressure of 2.5 MPa, and the data were analyzed using the software package ASTRA 7.14 to obtain the molecular weight.

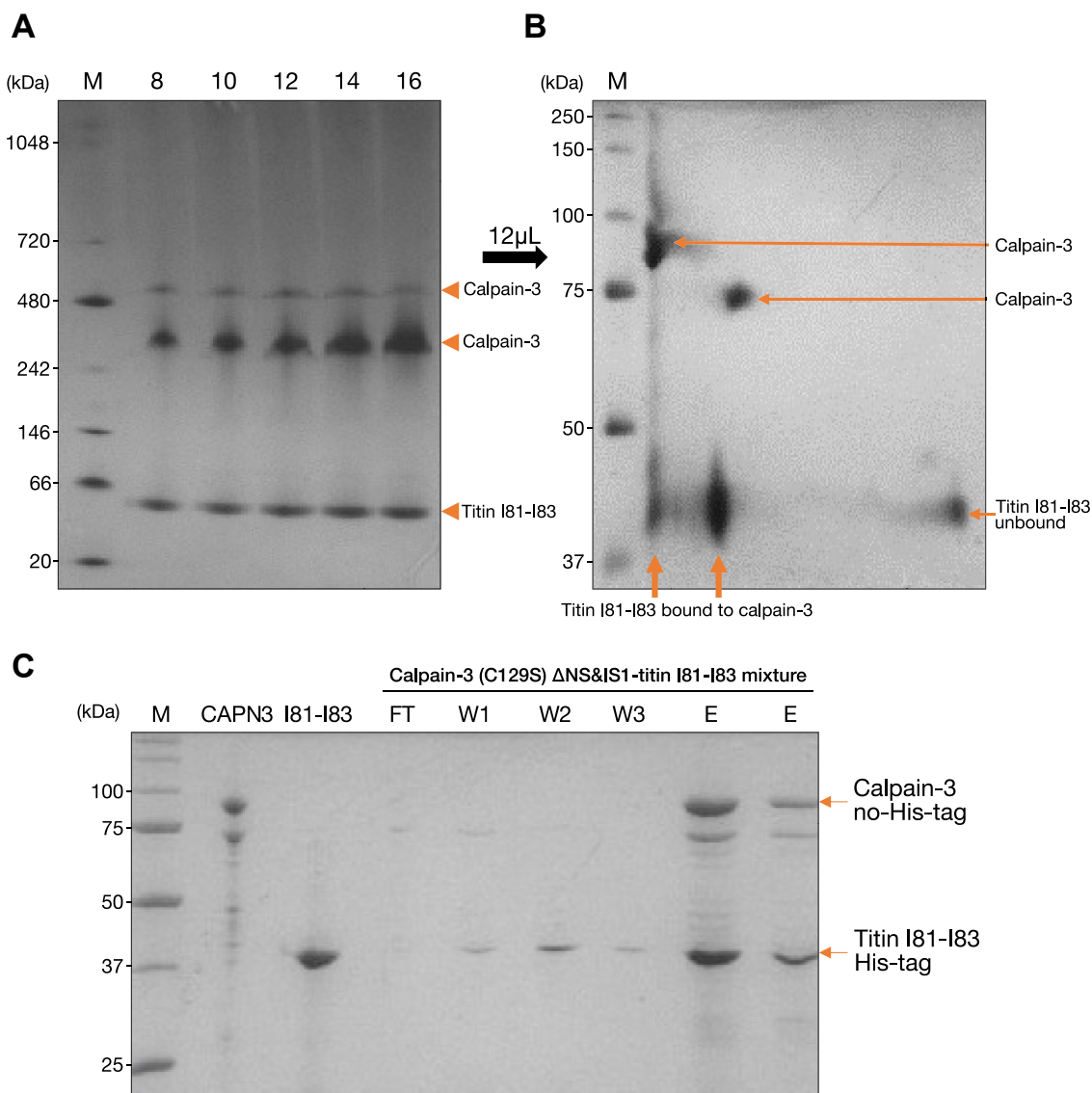


**Figure 12. Molecular mass analysis of calpain-3-titin I81-I83 complex by PAGE.** *A*, Blue Native PAGE: Lane M was loaded with the molecular mass markers with their masses indicated alongside the gel. Numbers above other lanes refer to the sample volume ( $\mu$ L) loaded. *B*, two-dimensional PAGE: A sample lane from (*A*) was soaked in SDS gel buffer and separated in the second dimension by SDS-PAGE. Arrows indicate the locations of calpain-3 and bound/unbound titin I81-I83 fragment. Lane M refers to the molecular mass markers for the second dimension of SDS-PAGE. *C*, pull-down assay for complex formation between calpain-3 (C129S)  $\Delta$ NS&IS1 and titin-I81-I83. Lane M: molecular mass markers. Lane CAPN3: calpain-3; Lane I81-I83: titin N2A region I81-I83 fragment. The remaining lanes are labeled as fractions from the Ni-agarose chromatography – FT: flow-through; W1, W2, and W3 are three wash fractions. Lanes E and E are two different loadings of the eluate.

### Sedimentation velocity analytical ultracentrifugation

Sedimentation velocity analytical ultracentrifugation experiments were performed at the Canadian Center for Hydrodynamics at the University of Lethbridge. To monitor mass action-driven reversible oligomerization, calpain-3 (C129A)  $\Delta$ NS&IS1 was measured at a high and low concentration. The high concentration (1.75  $\mu$ M) was measured at 280 nm in a buffer containing 20 mM Tris-HCl (pH 7.6), 100 mM NaCl, 2 mM EDTA, 5 mM TCEP, and 0.05% sodium azide. For the low concentration (0.30  $\mu$ M), which was measured at 225 nm, the buffer was diluted 10-fold with ddH<sub>2</sub>O to reduce the absorbance contributions of TCEP and EDTA at this wavelength. Both concentrations were measured at a speed of 34,000 rpm by UV intensity detection in a Beckman Optima

AUC analytical ultracentrifuge, using an An-60 Ti rotor and standard 2-channel epon centerpieces (Beckman-Coulter). Measurements were performed at 4 °C, and data were collected for 9 h. In addition, a low concentration sample (0.3  $\mu$ M) was cross-linked by treatment with 0.1% glutaraldehyde using a buffer containing 50 mM Tris-HCl buffer (pH 7.6), 25 mM NaCl, and 2 mM EDTA. The cross-linked calpain-3 sample was measured at 40,000 rpm to improve the separation of the different oligomeric states.

### Data analysis

Data were analyzed with UltraScan-III ver. 4.0, release 7034 (52). All data were processed as described in (53). Model-independent, diffusion-corrected integral sedimentation

## Calpain-3 homohexamer dissociates to dimers on binding titin

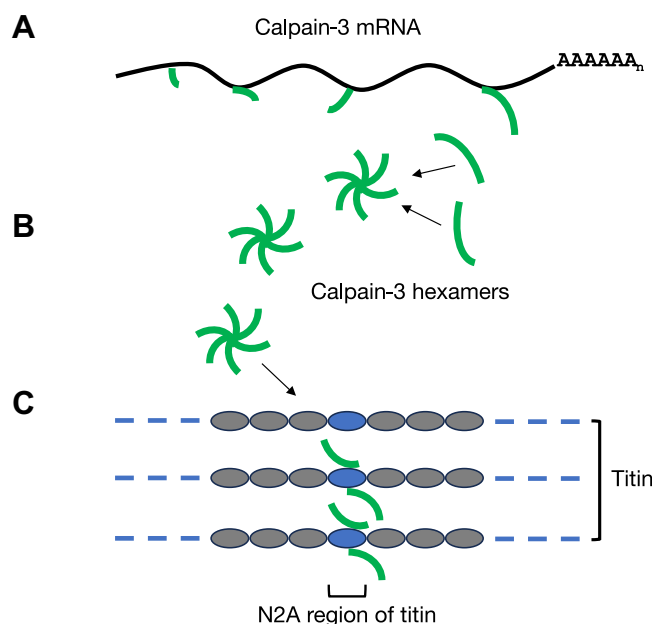


**Figure 13. Schematic model for calpain-3 deposition on titin.** A, calpain-3 (green line) is produced as a monomer by translation of its mRNA (black line with poly(A) tail) where its high local concentration favors oligomerization into a hexamer. B, calpain-3 hexamers transit to the sarcomere. C, on binding to the N2A region of the vertically aligned titin (indicated by the blue oval), the calpain-3 hexamer dissociates into dimers that bind to the high local concentration of the binding sites.

coefficient profiles were prepared with the enhanced van Holde–Weischet analysis (vHW) (54). To determine the molecular parameters of the stable oligomeric species, the data were modeled with the parametrically constrained spectrum analysis (55), enhanced by Monte Carlo analysis (56). An increasing sigmoid parameterization was found to produce the best fits. The partial specific volume of calpain-3 was assumed to be 0.729 ml/g based on its protein sequence as determined by UltraScan.

**Table 4**  
Statistics of single particle cryoEM data collection and processing

Data collection information	PNCC #160018	PNCC #160018	PNCC #160018
	Calpain-3	Calpain-3-I81-I83	Calpain-3-I81-I83
Microscopy		Thermo Fisher Scientific Krios G3i	
Detector		Gatan K3 with BioContinuum fringe-free energy filter	
Nominal magnification	105,000×	165,000×	165,000×
Voltage (kV)	300	300	300
Total electron dose ( $e^-/\text{Å}^2$ )	40.10107	36.2766	31.103019
Exposure time (s)	0.668	0.666	0.799
Nominal defocus range ( $\mu\text{m}$ )	2.0 (0.8–3.2)	1.5 (0.5–2.5)	1.8 (0.8–2.8)
Physical pixel size (super-res) ( $\text{Å}$ )	0.826 (0.413)	0.2556	0.507
Movies amount	6054	12,490	24,797
Frames	60	50	50
Single-particle reconstruction		EMDB-43646	
Software	CryoSPARC v4.2	CryoSPARC v4.2	
Number of micrographs contributed	4888	11,666	17,258
Initial particles picked	4,029,390	2,277,753	22,975,435
Particles refined	334,733	985,035	3,955,686
Initial model used	<i>Ab initio</i>		
Symmetry imposed	$D_3$		
Map overall resolution - FSC0.143 ( $\text{Å}$ )	3.85		
Applied b-factor ( $\text{Å}^2$ )	-190.5		

### BN-PAGE run in 1D and 2D

Calpain-3 (C129A)  $\Delta\text{NS}\&\text{IS1}$  (5.8  $\mu\text{M}$ ) or calpain-3 (C129A)  $\Delta\text{NS}\Delta\text{IS1}/\text{I81-I83}$  (38  $\mu\text{M}$ ) were mixed in 4X nondenaturing loading buffer [77.5 mM Tris-HCl (pH 6.8), 25% glycerol, and 0.05% bromophenol blue] and were separated on 4 to 16% Native PAGE Bis-Tris gradient gels (Thermo Fisher Scientific) (57). Following electrophoresis, protein bands were visualized by Coomassie Blue staining. For two-dimensional gel electrophoresis, the first-dimension was run under native conditions on BN-PAGE, then a strip of BN gel, which contained the complex bands, was subjected to the second dimension of SDS-PAGE. The protein spots on the 2D gel were visualized by Coomassie Blue staining.

### BioSAXS data collection

Biological small angle X-ray solution scattering experiments were performed on the BioSAXS beamline ID7A1 at Cornell MacCHESS. Calpain-3 (C129A)  $\Delta\text{NS}\&\text{IS1}$  was prepared at concentrations of 1.5 mg/ml or 3.0 mg/ml, in 20 mM Tris-HCl (pH 7.6), 100 mM NaCl, 2 mM EDTA, 2% glycerol, 0.05% sodium azide, and 10 mM 2-mercaptoethanol. Data were collected using an in-line Superdex 10/300 column equipped with an EIGER 4.0 detector. The beam energy range was 1.771203  $\text{Å}$ –0.885601  $\text{Å}$ . A series of 1096 images and 1359 images were collected from the 1.5 mg/ml and 3.0 mg/ml samples, respectively, with 2-s exposures per image. The BioXTAS RAW software (Version 2.1.1) (58) was used for data processing and preliminary analysis. Radiation damage was not observed in the samples. A summary of the SAXS parameters is given in Table 3.

### Molecular dynamics simulations for a homodimer structural model

A predicted structure of human calpain-3 lacking the NS and IS1 regions was generated by AlphaFold2 (42). The structure was duplicated and aligned through the complementary unpaired

fifth EF-hand motifs of the C-terminal PEF domains of the two calpain-3 molecules to match the crystal structure of the PEF homodimer association (PDB ID: 4OKH). Subsequently, this homodimer of calpain-3 was rendered in PyMOL (The PyMOL Molecular Graphics System, Version 2.0, Schrödinger, LLC) and subjected to molecular dynamics simulations using GROMACS (Version 2016.3) (59). Protein was solvated in a box containing 82,423 water molecules, 192 Na<sup>+</sup> ions, as well as 166 Cl<sup>-</sup> ions to neutralize the charge of the system. Energy minimization was performed using the steepest descents protocol, followed by position-restrained dynamics runs to equilibrate solvent and ions around the structure by constant-volume-temperature and constant-pressure-temperature, each 0.1 ns in duration. Finally, an unrestrained dynamics simulation was run for 100,000 steps over 20 ns at a temperature of 298 K.

### Preparation of single particle cryo-EM grids and screening

Cryo-EM grid preparation and sample screening were carried out in the Biomolecular Cryo-Electron Microscopy Facility, University of California. A freshly eluted aliquot (4  $\mu$ l) of calpain-3 (C129A)  $\Delta$ NS&IS1 (2.76 mg/ml) or calpain-3-titin/I81-I83 (2 mg/ml) from Superose 6 Increase 10/300 GL column chromatography was loaded onto glow-discharged holey carbon grids (Quantifoil 1.2/1.3 + 2 nm Carbon). The grids were blotted with filter paper for 2.5 s at 22 °C and then immediately plunged into liquid ethane cooled by liquid nitrogen using a Vitrobot Mark IV (Thermo Fisher Scientific). A sample of calpain-3 in complex with titin-I81-I83 from a pull-down experiment was also prepared, in which His-tagged titin I81-I83 was mixed as 'bait' with calpain-3 (C129S)  $\Delta$ NS&IS1 lacking its His-tag as 'prey' in a molar ratio of 10:1 with gentle agitation for 2.5 h at 4 °C. The mixture was then loaded onto a Ni-NTA affinity column followed by washing thoroughly with 20 mM Tris-HCl (pH 7.6), 100 mM NaCl, and 5 to 20 mM imidazole (wash buffer) until the eluate was protein-free as judged by the lack of reaction with Bradford dye reagent (Bio-Rad). The calpain-3-titin-I81-I83 complex was eluted with 300 mM imidazole in wash buffer. An aliquot (4  $\mu$ l) of the freshly eluted complex peak solution (4.0 mg/ml) was loaded onto glow-discharged holey carbon grids (Quantifoil 2/2). The procedures for blotting and plunge freezing the grids were the same as above. Evaluation of the vitreous samples was performed on a Glacios Cryo Transmission Electron Microscope (Thermo Fisher Scientific) operating at 200 kV and coupled to a Gatan K2 Summit direct electron detector at cryogenic temperatures.

### Single particle cryo-EM data acquisition and image processing

Cryo-EM single particle data were collected at the Pacific Northwest Center for Cryo-EM (PNCC – Portland, USA - PNCC #160018/160310) with SerialEM (60) on a Thermo Fisher Scientific Krios G3i microscope operating at 300 kV coupled to a Gatan K3 Direct Electron Detector and Bio-Continuum fringe-free energy filter. For calpain-3 data, the detector was used in super-resolution counting mode at a nominal magnification of 105,000 $\times$  which produced a final

pixel size of 0.413 Å. The total dose was 60 e<sup>-</sup>/Å<sup>2</sup>, over 60 frames with a nominal defocus range from -0.8 to -3.2  $\mu$ m. For two datasets of calpain-3 in complex with titin-I81-I83, a nominal magnification of 165,000 $\times$  was used, which resulted in a final pixel size of 0.256 Å and 0.507 Å, respectively. The total dose was 36.27 and 31.10 e<sup>-</sup>/Å<sup>2</sup>, over 50 frames, respectively with a nominal defocus range from -0.5 to -2.5 and -0.8 to -2.8  $\mu$ m, respectively. The data were processed using the CryoSPARC v4.2 workflow (61). In the pre-processing, all movie frames were first aligned to obtain a motion-corrected image by Patch Motion Correction followed by estimation of the Contrast Transfer Function. Next, for calpain-3 data, a total of 4,029,390 particles were automatically selected from 4888 micrographs and then used for template-free 2D classification. The best classes from 596,621 particles were subjected to 3D *ab initio* reconstruction followed by 3D classification. Particles in the best class (334,733 particles) were selected for 3D refinement using *D*<sub>3</sub> symmetry. In the post-processing, the final overall resolution FSC<sub>0.143</sub> of 3.85 Å was obtained after local and nonuniform refinement.

For the datasets of calpain-3 in complex with titin-I81-I83, totals of 2,277,753 and 22,975,435 particles were automatically selected from 11,666 and 17,258 micrographs, respectively, and subjected to template-free 2D classification. The best classes were selected from 985,035 and 3,955,686 particles, respectively. A summary of the single-particle cryo-EM statistics is given in Table 4.

### Model building and refinement

A sharpened cryo-EM map with a B-factor of -190.5 Å<sup>2</sup> was used for model building. A partial raw model was derived from ModelAngelo (45) as a reference, and fragments of the calpain-3 PEF domain from its crystal structure (PDB ID: 4OKH) were rigid-body docked into the map using UCSF Chimera/ChimeraX (44). Model fitting and refinement were done in Coot (62, 63).

### Data availability

All cryo-EM maps were deposited in the Electron Microscopy Data Bank (EMDB) under accession number EMDB-43646. Data collection details and model statistics are summarized in Tables 3 and 4. Additional data is available from the authors upon request.

---

*Supporting information*—This article contains supporting information.

*Acknowledgments*—We dedicate this manuscript to the memory of the late Professor Hiroyuki Sorimachi whose pioneering work on p94 (calpain-3) paved the way for this investigation. The Canadian Center of Hydrodynamics (CCH) at the University of Lethbridge was instrumental in performing sedimentation velocity analytic ultracentrifugation and subsequent analysis of calpain-3 samples with funding to BD from the Canada 150 Research Chairs Program (C150-2017-00015), Canada Foundation of Innovation (CFI-37589), Canadian Natural Science and Engineering Research

## Calpain-3 homohexamer dissociates to dimers on binding titin

Council (DG-RGPIN-2019-05637), NIH-NIGMS (1R01GM120600), NSF (TG-MCB070039N), and the University of Texas (TG457201). We thank Dr Omar Davulcu as well as Rose M. Haynes and the Pacific Northwest Center for CryoEM (PNCC) at Oregon Health & Science University for data collection and support on data processing. We also thank Drs. Irina Novikova and Craig Yoshioka at PNCC for data processing training and support at PNCC Compute. The authors also acknowledge the Biomolecular cryo-Electron Microscopy Facility at the Department of Chemistry and Biochemistry of the University of California - Santa Cruz (RRID:SCR\_021755) for scientific and technical assistance (NIH High-End Instrumentation program, S10OD02509). Molecular graphics and analyses performed with UCSF ChimeraX, developed by the Resource for Biocomputing, Visualization, and Informatics at the University of California, San Francisco, with support from National Institutes of Health R01-GM129325 and the Office of Cyber Infrastructure and Computational Biology, National Institute of Allergy and Infectious Diseases. This work was advanced by research conducted at the Center for High-Energy X-ray Sciences (CHEXS), which is supported by the National Science Foundation (BIO, ENG and MPS Directorates) under award DMR-1829070, and the Macromolecular Diffraction at CHESS (MacCHESS) facility, which is supported by award 1-P30-GM124166-01A1 from the National Institute of General Medical Sciences, National Institutes of Health, and by New York State's Empire State Development Corporation (NYSTAR). We are grateful to Dr Jeffery Lee for access to his SEC-MALS apparatus at the University of Toronto. We thank our colleagues Dr Mona Rahman, Dr Yasuko Ono, Mathias Bell and Thomas Hansen for their comments and edits on the manuscript.

**Author contributions**—Q. Y., A. H., B. D., V. H. B. S., and P. L. D. writing—review and editing; Q. Y. and P. L. D. writing—original draft; Q. Y., A. H., B. D., and V. H. B. S. visualization; Q. Y., A. H., B. D., V. H. B. S., and P. L. D. validation; Q. Y., A. H., V. H. B. S., and P. L. D. resources; Q. Y., A. H., B. D., and V. H. B. S. methodology; Q. Y., A. H., B. D., and V. H. B. S. investigation; Q. Y., A. H., B. D., and V. H. B. S. data curation; Q. Y., A. H., V. H. B. S., and P. L. D. conceptualization; B. D., V. H. B. S., and P. L. D. supervision; B. D. and V. H. B. S. software; B. D., V. H. B. S., and P. L. D. project administration; V. H. B. S. formal analysis; P. L. D. funding acquisition.

**Funding and additional information**—A portion of this research was supported by NIH grant U24GM129547 and performed at the PNCC at OHSU and accessed through EMSL (grid.436923.9), a DOE Office of Science User Facility sponsored by the Office of Biological and Environmental Research. Operational support was funded by a grant from the US Muscular Dystrophy Association (MDA577340) and by Foundation Award FRN 148422 from the Canadian Institutes of Health Research to P. L. D., who held the Canada Research Chair in Protein Engineering. The content is solely the responsibility of the authors and does not necessarily represent the official views of the National Institutes of Health.

**Conflict of interest statement**—The authors declare that they have no conflicts of interest with the contents of this article.

**Abbreviations**—The abbreviations used are: 2D, two-dimensional; BN-PAGE, Blue Native PAGE; CBSW, calpain-type beta-sandwich; IS, insertion sequence; LGMDR1, limb girdle muscular dystrophy

type R1; NS, N-terminal sequence; PC, protease core; PEF, penta-EF; SAXS, small angle X-ray light scattering; SEC-MALS, multi-angle light scattering coupled with size-exclusion chromatography.

### References

- Goll, D. E., Thompson, V. F., Li, H., Wei, W., and Cong, J. (2003) The calpain system. *Physiol. Rev.* **83**, 731–801
- Ono, Y., and Sorimachi, H. (2012) Calpains: an elaborate proteolytic system. *Biochim. Biophys. Acta* **1824**, 224–236
- Campbell, R. L., and Davies, P. L. (2012) Structure-function relationships in calpains. *Biochem. J.* **447**, 335–351
- Bertipaglia, I., and Carafoli, E. (2007) Calpains and human disease. *Subcell. Biochem.* **45**, 29–53
- Huang, Y., and Wang, K. K. (2001) The calpain family and human disease. *Trends Mol. Med.* **7**, 355–362
- Shapovalov, I., Harper, D., and Greer, P. A. (2022) Calpain as a therapeutic target in cancer. *Expert Opin. Ther. Targets* **26**, 217–231
- Spinuzzi, S., Albin, S., Best, H., and Richard, I. (2021) Calpains for dummies: what you need to know about the calpain family. *Biochim. Biophys. Acta Proteins Proteom.* **1869**, 140616
- Sorimachi, H., Imajoh-Ohmi, S., Emori, Y., Kawasaki, H., Ohno, S., Minami, Y., *et al.* (1989) Molecular cloning of a novel mammalian calcium-dependent protease distinct from both m- and mu-types. Specific expression of the mRNA in skeletal muscle. *J. Biol. Chem.* **264**, 20106–20111
- Richard, I., Broux, O., Allamand, V., Fougerousse, F., Chiannikulchai, N., Bourg, N., *et al.* (1995) Mutations in the proteolytic enzyme calpain 3 cause limb-girdle muscular dystrophy type 2A. *Cell* **81**, 27–40
- Kramerova, I., Beckmann, J. S., and Spencer, M. J. (2007) Molecular and cellular basis of calpainopathy (limb girdle muscular dystrophy type 2A). *Biochim. Biophys. Acta* **1772**, 128–144
- Kramerova, I., Kudryashova, E., Venkatraman, G., and Spencer, M. J. (2007) Calpain 3 participates in sarcomere remodeling by acting upstream of the ubiquitin-proteasome pathway. *Hum. Mol. Genet.* **16**, 1006
- Kramerova, I., Kudryashova, E., Wu, B., Ottenheijm, C., Granzier, H., and Spencer, M. J. (2008) Novel role of calpain-3 in the triad-associated protein complex regulating calcium release in skeletal muscle. *Hum. Mol. Genet.* **17**, 3271–3280
- Ojima, K., Kawabata, Y., Nakao, H., Nakao, K., Doi, N., Kitamura, F., *et al.* (2010) Dynamic distribution of muscle-specific calpain in mice has a key role in physical-stress adaptation and is impaired in muscular dystrophy. *J. Clin. Invest.* **120**, 2672–2683
- Murphy, R. M. (2010) Calpains, skeletal muscle function and exercise. *Clin. Exp. Pharmacol. Physiol.* **37**, 385–391
- Elce, J. S., Davies, P. L., Hegadorn, C., Maurice, D. H., and Arthur, J. S. (1997) The effects of truncations of the small subunit on m-calpain activity and heterodimer formation. *Biochem. J.* **326**, 31–38
- Moldoveanu, T., Hosfield, C. M., Lim, D., Elce, J. S., Jia, Z., and Davies, P. L. (2002) A Ca(2+) switch aligns the active site of calpain. *Cell* **108**, 649–660
- Lin, G. D., Chattopadhyay, D., Maki, M., Wang, K. K., Carson, M., Jin, L., *et al.* (1997) Crystal structure of calcium bound domain VI of calpain at 1.9 Å resolution and its role in enzyme assembly, regulation, and inhibitor binding. *Nat. Struct. Biol.* **4**, 539–547
- Blanchard, H., Grochulski, P., Li, Y., Arthur, J. S., Davies, P. L., Elce, J. S., *et al.* (1997) Structure of a calpain Ca(2+)-binding domain reveals a novel EF-hand and Ca(2+)-induced conformational changes. *Nat. Struct. Biol.* **4**, 532–538
- Hosfield, C. M., Elce, J. S., Davies, P. L., and Jia, Z. (1999) Crystal structure of calpain reveals the structural basis for Ca(2+)-dependent protease activity and a novel mode of enzyme activation. *EMBO J.* **18**, 6880–6889
- Strobl, S., Fernandez-Catalan, C., Braun, M., Huber, R., Masumoto, H., Nakagawa, K., *et al.* (2000) The crystal structure of calcium-free human m-calpain suggests an electrostatic switch mechanism for activation by calcium. *Proc. Natl. Acad. Sci. U. S. A.* **97**, 588–592

21. Sorimachi, H., Ohmi, S., Emori, Y., Kawasaki, H., Saido, T. C., Ohno, S., *et al.* (1990) A novel member of the calcium-dependent cysteine protease family. *Biol. Chem. Hoppe Seyler* **371**, 171–176
22. Kinbara, K., Sorimachi, H., Ishiura, S., and Suzuki, K. (1998) Skeletal muscle-specific calpain, p49: structure and physiological function. *Biochem. Pharmacol.* **56**, 415–420
23. Sorimachi, H., Toyama-Sorimachi, N., Saido, T. C., Kawasaki, H., Sugita, H., Miyasaka, M., *et al.* (1993) Muscle-specific calpain, p94, is degraded by autolysis immediately after translation, resulting in disappearance from muscle. *J. Biol. Chem.* **268**, 10593–10605
24. Sorimachi, H., Hata, S., and Ono, Y. (2011) Calpain chronicle—an enzyme family under multidisciplinary characterization. *Proc. Jpn. Acad. Ser. B Phys. Biol. Sci.* **87**, 287–327
25. Tompa, P. (2002) Intrinsically unstructured proteins. *Trends Biochem. Sci.* **27**, 527–533
26. Diaz, B. G., Moldoveanu, T., Kuiper, M. J., Campbell, R. L., and Davies, P. L. (2004) Insertion sequence 1 of muscle-specific calpain, p94, acts as an internal propeptide. *J. Biol. Chem.* **279**, 27656–27666
27. Rey, M. A., and Davies, P. L. (2002) The protease core of the muscle-specific calpain, p94, undergoes Ca<sup>2+</sup>-dependent intramolecular autolysis. *FEBS Lett.* **532**, 401–406
28. Ye, Q., Campbell, R. L., and Davies, P. L. (2018) Structures of human calpain-3 protease core with and without bound inhibitor reveal mechanisms of calpain activation. *J. Biol. Chem.* **293**, 4056–4070
29. McCartney, C. E., Ye, Q., Campbell, R. L., and Davies, P. L. (2018) Insertion sequence 1 from calpain-3 is functional in calpain-2 as an internal propeptide. *J. Biol. Chem.* **293**, 17716–17730
30. Sorimachi, H., Kinbara, K., Kimura, S., Takahashi, M., Ishiura, S., Sasagawa, N., *et al.* (1995) Muscle-specific calpain, p94, responsible for limb girdle muscular dystrophy type 2A, associates with connectin through IS2, a p94-specific sequence. *J. Biol. Chem.* **270**, 31158–31162
31. Kinbara, K., Sorimachi, H., Ishiura, S., and Suzuki, K. (1997) Muscle-specific calpain, p94, interacts with the extreme C-terminal region of connectin, a unique region flanked by two immunoglobulin C2 motifs. *Arch. Biochem. Biophys.* **342**, 99–107
32. Hayashi, C., Ono, Y., Doi, N., Kitamura, F., Tagami, M., Mineki, R., *et al.* (2008) Multiple molecular interactions implicate the connectin/titin N2A region as a modulating scaffold for p94/calpain 3 activity in skeletal muscle. *J. Biol. Chem.* **283**, 14801–14814
33. Kinbara, K., Ishiura, S., Tomioka, S., Sorimachi, H., Jeong, S. Y., Amano, S., *et al.* (1998) Purification of native p94, a muscle-specific calpain, and characterization of its autolysis. *Biochem. J.* **335**, 589–596
34. Ravulapalli, R., Diaz, B. G., Campbell, R. L., and Davies, P. L. (2005) Homodimerization of calpain 3 penta-EF-hand domain. *Biochem. J.* **388**, 585–591
35. Partha, S. K., Ravulapalli, R., Allingham, J. S., Campbell, R. L., and Davies, P. L. (2014) Crystal structure of calpain-3 penta-EF-hand (PEF) domain - a homodimerized PEF family member with calcium bound at the fifth EF-hand. *FEBS J.* **281**, 3138–3149
36. Hata, S., Doi, N., Shinkai-Ouchi, F., and Ono, Y. (2020) A muscle-specific calpain, CAPN3, forms a homotrimer. *Biochim. Biophys. Acta Proteins Proteom.* **1868**, 140411
37. Maki, M., Kitaura, Y., Satoh, H., Ohkouchi, S., and Shibata, H. (2002) Structures, functions and molecular evolution of the penta-EF-hand Ca<sup>2+</sup>-binding proteins. *Biochim. Biophys. Acta* **1600**, 51–60
38. Konarev, P. V., Volkov, V. V., Sokolova, A. V., Koch, M. H. J., and Svergun, D. I. (2003) PRIMUS: a Windows PC-based system for small-angle scattering data analysis. *J. Appl. Crystallogr.* **36**, 1277–1282
39. Svergun, D. (1992) Determination of the regularization parameter in indirect-transform methods using perceptual criteria. *J. Appl. Crystallogr.* **25**, 495–503
40. Franke, D., Petoukhov, M. V., Konarev, P. V., Panjkovich, A., Tuukkanen, A., Mertens, H. D. T., *et al.* (2017) Atsas 2.8: a comprehensive data analysis suite for small-angle scattering from macromolecular solutions. *J. Appl. Crystallogr.* **50**, 1212–1225
41. Svergun, D. I. (1999) Restoring low resolution structure of biological macromolecules from solution scattering using simulated annealing. *Biophys. J.* **76**, 2879–2886
42. Jumper, J., Evans, R., Pritzel, A., Green, T., Figurnov, M., Ronneberger, O., *et al.* (2021) Highly accurate protein structure prediction with AlphaFold. *Nature* **596**, 583–589
43. Svergun, D., Barberato, C., and Koch, M. H. J. (1995) Crysol - a program to evaluate X-ray solution scattering of biological macromolecules from atomic coordinates. *J. Appl. Crystallogr.* **28**, 768–773
44. Pettersen, E. F., Goddard, T. D., Huang, C. C., Couch, G. S., Greenblatt, D. M., Meng, E. C., *et al.* (2004) UCSF Chimera—a visualization system for exploratory research and analysis. *J. Comput. Chem.* **25**, 1605–1612
45. [preprint] Jamali, K., Kall, L., Zhang, R., Brown, A., Kimanius, D., and Scheres, S. H. W. (2023) Automated model building and protein identification in cryo-EM maps. *bioRxiv*. <https://doi.org/10.1101/2023.05.16.541002>
46. Murphy, R. M., and Lamb, G. D. (2009) Calpain-3 is activated following eccentric exercise. *J. Appl. Physiol.* (1985) **106**, 2068
47. Stronczek, C., Lange, S., Bullard, B., Wolniak, S., Borgeson, E., Mayans, O., *et al.* (2021) The N2A region of titin has a unique structural configuration. *J. Gen. Physiol.* **153**, e202012766
48. Kretsinger, R. H. (1997) EF-hands embrace. *Nat. Struct. Biol.* **4**, 514–516
49. Leinala, E. K., Arthur, J. S., Grochulski, P., Davies, P. L., Elce, J. S., and Jia, Z. (2003) A second binding site revealed by C-terminal truncation of calpain small subunit, a penta-EF-hand protein. *Proteins* **53**, 649–655
50. Elce, J. S., Hegadorn, C., Gauthier, S., Vince, J. W., and Davies, P. L. (1995) Recombinant calpain II: improved expression systems and production of a C105A active-site mutant for crystallography. *Protein Eng.* **8**, 843–848
51. McCartney, C. E., and Davies, P. L. (2019) Bacterial expression and purification of calpains. *Methods Mol. Biol.* **1915**, 13–27
52. Demeler, B., and Gorbet, G. (2016) *Analytical Ultracentrifugation Data Analysis with UltraScan-III*. Springer, Tokyo: 119–143
53. Demeler, B. (2024) Methods for the design and analysis of analytical ultracentrifugation experiments. *Curr. Protoc.* **4**, e974
54. Demeler, B., and van Holde, K. E. (2004) Sedimentation velocity analysis of highly heterogeneous systems. *Anal. Biochem.* **335**, 279–288
55. Gorbet, G., Devlin, T., Hernandez Uribe, B. I., Demeler, A. K., Lindsey, Z. L., Ganji, S., *et al.* (2014) A parametrically constrained optimization method for fitting sedimentation velocity experiments. *Biophys. J.* **106**, 1741–1750
56. Demeler, B., and Brookes, E. (2008) Monte Carlo analysis of sedimentation experiments. *Colloid Polym. Sci.* **286**, 129–137
57. Fiala, G. J., Schamel, W. W., and Blumenthal, B. (2011) Blue native polyacrylamide gel electrophoresis (BN-PAGE) for analysis of multi-protein complexes from cellular lysates. *J. Vis. Exp.* <https://doi.org/10.3791/2164>
58. Hopkins, J. B., Gillilan, R. E., and Skou, S. (2017) BioXTAS RAW: improvements to a free open-source program for small-angle X-ray scattering data reduction and analysis. *J. Appl. Crystallogr.* **50**, 1545–1553
59. Rakhshani, H., Dehghanian, E., and Rahati, A. (2019) Enhanced GRO-MAACS: toward a better numerical simulation framework. *J. Mol. Model.* **25**, 355
60. Mastronarde, D. N. (2005) Automated electron microscope tomography using robust prediction of specimen movements. *J. Struct. Biol.* **152**, 36–51
61. Punjani, A., Rubinstein, J. L., Fleet, D. J., and Brubaker, M. A. (2017) cryoSPARC: algorithms for rapid unsupervised cryo-EM structure determination. *Nat. Methods* **14**, 290–296
62. Emsley, P., and Cowtan, K. (2004) Coot: model-building tools for molecular graphics. *Acta Crystallogr. D Biol. Crystallogr.* **60**, 2126–2132
63. Casanal, A., Lohkamp, B., and Emsley, P. (2020) Current developments in Coot for macromolecular model building of electron cryo-microscopy and crystallographic data. *Protein Sci.* **29**, 1069–1078